Intramolecular Charge Transfer with the Planarized 4-Cyanofluorazene and Its Flexible Counterpart 4-Cyano-*N*-phenylpyrrole. Picosecond Fluorescence Decays and Femtosecond Excited-State Absorption

Sergey I. Druzhinin,[§,†] Sergey A. Kovalenko,[*,‡] Tamara A. Senyushkina,[§] Attila Demeter,[⊥] Reinhard Machinek,[#] Mathias Noltemeyer,[+] and Klaas A. Zachariasse[*,§]

Max-Planck-Institut für biophysikalische Chemie, Spektroskopie and Photochemische Kinetik, 37070 Göttingen, Germany, Institut für Chemie, Humboldt Universität zu Berlin, Brook-Taylor Strasse 2, 12489 Berlin, Germany, Institute of Materials and Environmental Chemistry, Chemical Research Center, Hungarian Academy of Sciences. P. O. Box 17, 1525 Budapest, Hungary, Institut für Organische Chemie, Universität Göttingen, Tammannstrasse 2, 37077 Göttingen, Germany, and Institut für Anorganische Chemie, Universität Göttingen, Tammannstrasse 2, 37077 Göttingen, Germany

Received: April 29, 2008; Revised Manuscript Received: June 13, 2008

The fluorescence spectrum of the rigidified 4-cyanofluorazene (FPP4C) in *n*-hexane consists of a dual emission from a locally excited (LE) and an intramolecular charge-transfer (ICT) state, with an ICT/LE fluorescence quantum yield ratio of $\Phi'(\mathrm{ICT})/\Phi(\mathrm{LE}) = 3.3$ at 25 °C. With the flexible 4-cyano-*N*-phenylpyrrole (PP4C) in *n*-hexane, such an ICT reaction also takes place, with $\Phi'(\mathrm{ICT})/\Phi(\mathrm{LE}) = 1.5$, indicating that for this reaction, a perpendicular twist of the pyrrole and benzonitrile moieties is not required. The ICT emission band of FPP4C and PP4C in *n*-hexane has vibrational structure, but a structureless band is observed in all other solvents more polar than the alkanes. The enthalpy difference ΔH of the LE → ICT reaction in *n*-hexane, −11 kJ/mol for FPP4C and −7 kJ/mol for PP4C, is determined by analyzing the temperature dependence of $\Phi'(\mathrm{ICT})/\Phi(\mathrm{LE})$. Using these data, the energy $E(\mathrm{FC,ICT})$ of the Franck−Condon ground state populated by the ICT emission is calculated, 41 (FPP4C) and 40 kJ/mol (PP4C). These large values for $E(\mathrm{FC,ICT})$ lead to the conclusion that with FPP4C and PP4C, direct ICT excitation, bypassing LE, does not take place. FPP4C has an ICT dipole moment of 15 D, similar to that of PP4C (16 D). Picosecond fluorescence decays allow the determination of the ICT lifetime, from which the radiative rate constant $k'_f(\mathrm{ICT})$ is derived, with comparable values for FPP4C and PP4C. This shows that an argument for a twisted ICT state of PP4C cannot come from $k'_f(\mathrm{ICT})$. After correction for the solvent refractive index and the energy of the emission maximum $\tilde{\nu}^{\max}(\mathrm{ICT})$, it appears that $k'_f(\mathrm{ICT})$ is solvent-polarity-independent. Femtosecond transient absorption with FPP4C and PP4C in *n*-hexane reveals that the ICT state is already nearly fully present at 100 fs after excitation, in rapid equilibrium with LE. In MeCN, the ICT state of FPP4C and PP4C is likewise largely developed at this delay time, and the reaction is limited by dielectric solvent relaxation, which shows that the ICT reaction is ultrafast, at the experimental time limit of 50 fs. PP4C and FPP4C have a similar planar ICT structure, without an appreciable twist of the pyrrole and benzonitrile subgroups. Their crystal structure is compared with calculations for the S_0 ground state.

Introduction

In the discussion of intramolecular charge transfer (ICT) with aminobenzonitriles and *N*-phenylpyrroles in the excited singlet state, the structure of these electron donor (D)/acceptor (A) molecules, in the S_0 ground state and especially in the locally excited (LE) and ICT states, has played an important role. Whereas direct experimental information on the S_0 structure of these D/A compounds can be deduced from X-ray crystal analysis,[1–3] such information on the ICT state is only available for crystalline 4-(diisopropylamino)benzonitrile (DIABN).[4,5] It was concluded from these studies that the amino group has a twist angle of 10° with respect to the benzonitrile moiety, that is, the ICT state of DIABN is effectively planar. Recently, the interpretation of these femtosecond X-ray measurements of DIABN crystal powder has been questioned on the basis of experiments in which the ICT state of DIABN was claimed to be prepared by direct excitation of the crystal powder with 400 nm laser light, an excitation with an energy of around 6000 cm^{-1} below that of S_1.[6] Under such strongly endothermic conditions, an anti-Stokes process, S_1 can normally only be populated by two-photon absorption.[7,8]

A more common and simple experimental approach to obtain structural information on the various intermediates involved in ICT reactions has been the use of model compounds, for which the structure is assumed to be known. Examples of such model substances for the planar LE state of 4-(dimethylamino)benzonitrile (DMABN) are 1-methyl-5-cyanoindoline (NMC5) and 1-methyl-6-cyano-1,2,3,4-tetrahydroquinoline (NMC6), whereas

* To whom correspondence should be addressed. E-mail: S.A.K., skovale@chemie.hu-berlin.de; K.A.Z., kzachar@gwdg.de. Fax: +49-551-201-1501.

† Max-Planck-Institut für biophysikalische Chemie, Spektroskopie und Photochemische Kinetik.

§ Affiliation: Chemistry Department, Moscow State University, 119992 Moscow, Russia.

‡ Humboldt Universität zu Berlin.

⊥ Hungarian Academy of Sciences.

Institut für Organische Chemie, Universität Göttingen.

+ Institut für Anorganische Chemie, Universität Göttingen.

10.1021/jp8037413 CCC: $40.75
Published on Web 08/16/2008

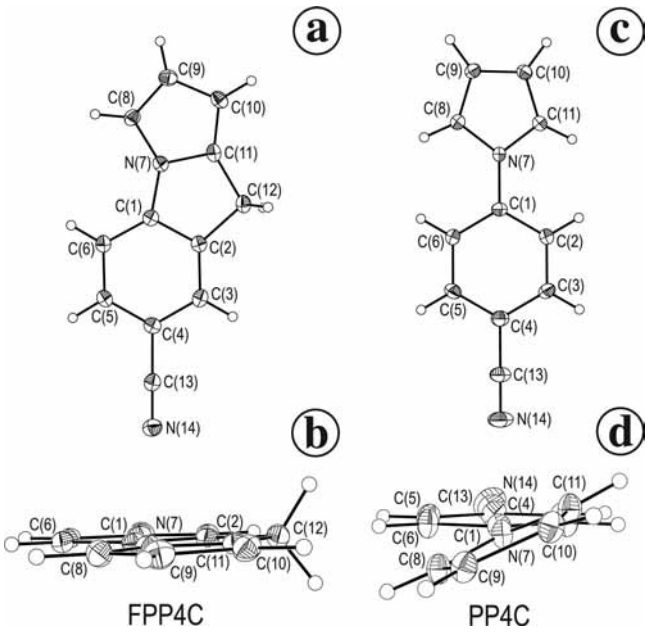

Figure 1. Crystal structures of 4-cyanofluorazene (FPP4C) (left) and 4-cyano-*N*-phenylpyrrole (PP4C) (right). For both molecules, a view from above (a and c) and one along the axis from the pyrrole nitrogen to the cyano group (b and d) are presented. The amino twist angle θ is defined as (C(2)C(1)N(7)C(11) + C(6)C(1)N(7)C(8))/2. The pyramidal angle φ is the angle between the vector N(7)C(1) and the plane through C(8)N(7)C(11).

CHART 1

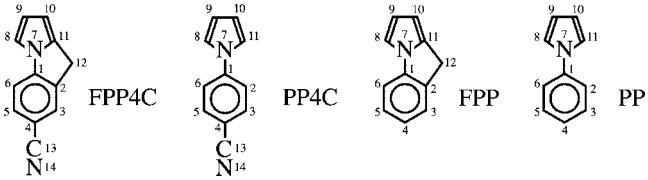

3,5-dimethyl-4-(dimethylamino)benzonitrile (MMD) has been employed as a model for a twisted ICT state.[9]

A problem arises, however, in the interpretation of the significance of the experiments with these model compounds.[10] Because ICT only occurs with D/A systems having a sufficiently small energy gap $\Delta E(S_1,S_2)$ between the two lowest excited singlet states (the PICT model),[11–14] the structural difference between a molecule undergoing ICT and its synthetically modified model compound can lead to substantial differences in $\Delta E(S_1,S_2)$ and hence in the ability to undergo an ICT reaction. This is, for example, the case with the pair DMABN and NMC6, for which the absence of ICT with NMC6 is not related to its planar molecular structure but is caused by a too large $\Delta E(S_1,S_2)$.[10] As a support of this interpretation, it was found that ICT readily occurs by replacing the *N*-methyl group of NMC6 by a *tert*-butyl substituent, 1-*tert*-butyl-6-cyano-1,2,3,4-tetrahydroquinoline (NTC6). With NTC6, $\Delta E(S_1,S_2)$ is considerably smaller than it is for NMC6, making efficient ICT possible.[10,15] The effective planarity of NTC6 in the ICT state has been questioned on the basis of recent calculations.[16–18]

Besides the 4-(dialkylamino)benzonitriles such as DMABN and NTC6, also *N*-phenylpyrrole (PP)[9,19–21] and 4-cyano-*N*-phenylpyrrole (PP4C)[9,22–25] undergo an ICT reaction. For the ICT state of PP4C, a configuration with perpendicularly twisted (TICT) pyrrole and benzonitrile moieties was postulated because of the strongly forbidden ICT emission,[25] although a planar ICT structure was suggested[9,22] in earlier publications.

The model compound approach used in the comparison of DMABN and NTC6 has also been adopted to investigate the structure of the ICT state of PP. With fluorazene (FPP), in which twisting of the pyrrole and phenyl subgroups is prevented by a methylene linker, fast and efficient ICT takes place in polar solvents such as acetonitrile (MeCN), similar to what was found for the flexible parent molecule PP.[26] It was hence concluded that the ICT state of PP is in fact planar and that a perpendicular twist of the donor group is not required for the occurrence of ICT. The same conclusion was made for the aminobenzonitriles, on the basis of the ICT reaction observed with NTC6, as discussed above.[10,15] Calculations on fluorazene find the expected planar ICT state but compute a fully twisted ICT state for PP,[27,28] in contradiction with our conclusions. In one of these calculations,[27] the phenyl ring of FPP and PP remains planar in the ICT state, whereas in the other,[28] the phenyl ring of these molecules has lost its planarity due to the pyramidal character of the ring carbon to which the pyrrole group is attached. A similar conclusion was reached in calculations on DMABN.[16,17]

With FPP and PP, ICT is not detected in nonpolar and low-polarity solvents such as *n*-hexane and diethyl ether (DEE) but only takes place in solvents more polar than DEE, for example, in tetrahydrofuran (THF) and MeCN.[19,20] With PP4C, in contrast, efficient ICT is found in all solvents investigated, from the nonpolar perfluoromethylcyclohexane (pFMCH) and *n*-hexane to the strongly polar MeCN and methanol.[21–26] Therefore, the rigidified compound 4-cyano-*N*-phenylpyrrole (FPP4C) was synthesized, with a $-CH_2-$ bridge between the pyrrole and benzonitrile subgroups. The results of photostationary and picosecond time-resolved fluorescence experiments together with femtosecond transient absorption measurements are presented here. Studies with the flexible counterpart PP4C were carried out for comparison.

Experimental Section

9*H*-Pyrrolo[1,2-*a*]indole-7-carbonitrile (4-cyanofluorazene, FPP4C) was synthesized as follows. 2-Amino-5-bromo-benzoic acid (Aldrich) was reacted with 2,5-dimethoxytetrahydrofuran (Aldrich) in acetic acid, giving 5-bromo-2-(1H-pyrrole-1-yl)benzoic acid.[29] This product was treated with PCl_5 in toluene. After addition of $SnCl_4$,[30] 7-bromo-9H-pyrrolo-[1,2-a]indole-9-one was obtained, which was added to a solution of semicarbazide hydrochloride (Aldrich) in ethanol and refluxed for 6 h to give the semicarbazone. This compound together with KOH was heated to 210 °C in diethylene glycol, resulting under evolution of nitrogen in 7-bromo-9*H*-pyrrolo-[1,2-*a*]indole (4-bromofluorazene). Finally, FPP4C (mp 146.8−148.0°) was made from 4-bromofluorazene and CuCN in *N*,*N*-dimethylacetamide by employing microwave irradiation (CEM Discover).

^{1}H NMR (600 MHz, $CDCl_3$, in ppm): FPP4C, 3.85 (s(br), 2H12), 6.15 (ddt, H10, $J_{10,9} = 3.31$ Hz, $J_{10,8} = 1.03$ Hz, $J_{10,12} = 1.47$ Hz), 6.43 (dd, H9, $J_{9,10} = 3.31$ Hz, $J_{9,8} = 2.90$ Hz), 7.09 (ddt, H8, $J_{8,9} = 2.90$ Hz, $J_{8,10} = 1.03$ Hz, $J_{8,12} = 0.88$ Hz), 7.28 (dd, H6, $J_{6,5} = 7.99$ Hz, $J_{6,3} = 0.60$ Hz, $J_{6,12} = 0.40$ Hz), 7.62 (ddt, H5, $J_{5,6} = 7.99$ Hz, $J_{5,3} = 1.60$ Hz, $J_{5,12} = 0.68$ Hz), 7.63 (ddt, H3, $J_{3,5} = 1.60$ Hz, $J_{3,6} = 0.60$ Hz); PP4C, 6.39 (m, BB′, H8,H11), 7.12 (m, AA′, H9,H10), 7.46 (m, AA′, H2,H6), 7.70 (m, BB′, H3,H5). ^{13}C NMR (500 MHz, $CDCl_3$, in ppm): FPP4C, 28.7 (C12), 103.0 (C10), 106.1 (C4), 110.1 (C6), 110.3 (C8), 115.1 (C9), 119.2 (C13), 129.3 (C3), 132.9 (C5), 135.6 (C11), 136.0 (C2), 144.3 (C1); PP4C, 108.6 (C4), 112.2 (C9,C10), 118.5 (C13), 118.9 (C8,C11), 119.9 (C2,C6), 133.8 (C3,C5), 143.7 (C1).

The synthesis of FPP, similar to that of FPP4C, has been reported previously.[26] The purification of FPP4C, FPP, and PP4C (Maybridge) was carried out as described before.[15] All solvents were chromato-

TABLE 1: Data for the Ground-State Structures of FPP4C, PP4C, FPP, and PP from X-ray Crystal Analysis (exp) and from Calculations (calc)[a]

	FPP4C exp	PP4C exp[b]	PP4C exp[c]	PP4C calc[c]	FPP calc[d,e]	FPP calc[f,g]	PP exp[h]	PP calc[d,e,i]	PP calc[g,h,i]
N(7)−C(1)	139.9	140.7	140.6	141.0	139.7	139.6	142.3	141.3	141.5
N(7)−C(8)	138.5	137.9	138.2	138.9	136.8	136.6	137.9	137.5	137.3
N(7)−C(11)	138.2	137.9	138.2	138.9	137.4	137.0	137.9	137.5	137.3
C(1)−C(2)	139.8	139.4	139.0	140.6	140.5	138.1	139.4	139.8[b]	139.6
C(1)−C(6)	138.4	139.4	139.0	140.6	138.5	138.1	139.4	139.8	139.2
C(2)−C(3)	138.1	138.5	138.8	139.1	138.5	138.1	138.9	139.5	139.1
C(3)−C(4)	140.6	139.6	138.9	139.1	140.5	140.1	138.8	139.5	139.1
C(4)−C(5)	140.0	139.6	138.9	140.7	139.3	139.6	138.8	139.5	139.2
C(5)−C(6)	139.3	138.5	138.8	140.7	140.3	139.9	138.9	139.5	139.6
C(8)−C(9)	136.7	137.0	135.5	137.6	137.3	137.4	136.2	136.9	137.1
C(9)−C(10)	142.3	140.8	141.1	143.0	143.7	143.7	141.2	142.9	143.2
C(10)−C(11)	135.9	137.0	135.5	137.6	136.8	136.8	136.2	136.9	137.1
C(11)−C(12)	150.8				150.9	151.0			
C(2)−C(12)	152.2				152.3	152.3			
C(4)−C(13)	144.1	143.2	144.6	143.5					
C(13)−N(14)	115.0	114.7	111.6	116.5					
C(1)−N(7)−C(8)	112.0	125.7	126.2	125.8	111.7[d]	138.1[f]	126.3	125.8[d]	125.7[f]
C(1)−N(7)−C(11)	137.9	125.7	126.2	125.8	110.1[d]	111.7[f]	125.8	125.8[d]	125.6[f]
C(8)−N(7)−C(11)	110.1	108.6	107.5	108.5	138.2[d]	110.3[f]	107.9	108.4[d]	108.7[f]
ΣN^j	360.0	360.0	360	360	360	360	360.0	360.0	360
twist angle θ^k	1.0	24.2	24.0	30.9	0	0	5.7	42.7	39.4
pyramidal angle φ^l	0.2	0.0	0.0	0.0	0.0[d]	0.1[f]	0.3	0.0[d]	0.1[f]
quinoidality[m]	0.9950	0.9921	0.9993	1.000	1.007	1.002	1.001	1.000	1.003

[a] See atom numbering in Chart 1 and Figure 1. The bond lengths are in picometers (pm), and the angles are in degree. [b] Data from ref 36. [c] Data from ref 37 (calc: DFT). [d] Data from ref 27 (CASSCF). [e] Private communication from Prof. Cao (ref 27). [f] Data from ref 28 (CASSCF)). [g] Private communication from Prof. Li and Dr. He (ref 28). [h] Data from ref 20. [i] For earlier computations, see ref 20. [j] Sum of the angles around the pyrrole nitrogen (Figure 1). [k] Twist angle θ: (C(6)C(1)N(7)C(8) + C(6)C(1)N(7)C(11))/2 (Figure 1). [l] Pyramidal angle φ: angle between the vector N(7)C(1) and the plane C(8)N(7)C(11) (Figure 1). [m] Quinoidality: (C(5) − C(6))/(C(4) − C(5)) (Figure 1).

TABLE 2: Data Obtained from the Fluorescence and Absorption Spectra of FPP4C and PP4C in *n*-Hexane and Acetonitrile (MeCN)

	FPP4C				PP4C			
solvent	*n*-hexane		MeCN		*n*-hexane		MeCN	
T [°C]	25	−95	25	−45	25	−95	25	−45
Φ(LE)	0.097		0[a]	0[a]	0.050		0[a]	0[a]
Φ′(ICT)	0.324		0.253	0.307	0.075		0.064	0.067
Φ′(ICT)/Φ(LE)	3.3	68			1.5	11		
Φ(ISC)[b]	0.48	−	0.44	−	0.59	−	0.63	−
ΔH [kJ/mol][c]	−11				−7			
$\tilde{\nu}^{max}$ (total,fl) [cm^{-1}]	28 670	28 460	21 550	21 040	29 960	29 470	20 750	20 080
$\tilde{\nu}^{max}$(ICT) [cm^{-1}]	28 000	28 460	21 550	21 040	29 030	29 450	20 750	20 080
$\tilde{\nu}^{max}$(LE) [cm^{-1}]	30 610	30 580	−	−	31 350	31 410	−	−
$\tilde{\nu}^{max}$(abs) [cm^{-1}]	33 660	33 550	34 140	34 020	34 990	34 640	35 180	34 990
ε^{max} [M^{-1} cm^{-1}]	22 600		23 820		22 550		24 000	
$E(S_1)$ [cm^{-1}][d]	32 400	32 010	28 740	27 900	33 280	32 860	28 870	27 720
$\Delta E(S_1,S_2)$ [cm^{-1}][e]	1260				1710			
E(FC,ICT) [kJ/mol][f]	41				40			

[a] Total fluorescence spectrum consists of ICT emission. LE emission could not be detected. [b] Measurements as in ref 20. [c] Enthalpy difference between LE and ICT, determined from a plot of ln(Φ′(ICT)/Φ(LE)) vs 1000/T (eq 2). [d] Crossing point of the fluorescence and absorption spectra (Figures 2−5). [e] The energy difference $\tilde{\nu}^{max}$(abs) − $E(S_1)$ is taken as an approximation for the energy gap $\Delta E(S_1,S_2)$ between the two lowest excited singlet states (ref 3). [f] Energy of the Franck−Condon (FC) state reached upon ICT emission. E(FC,ICT) = $E(S_1)$ + (ΔH) − $\tilde{\nu}^{max}$(ICT), eq 3.

graphed over Al_2O_3 just prior to use. The solutions, with an optical density between 0.4 and 0.6 for the maximum of the first band in the absorption spectrum, were deaerated by bubbling with nitrogen for 15 min. The measurement and treatment of the fluorescence spectra, quantum yields, and single-photon counting (SPC) decays and also that of the femtosecond transient absorption spectra have been described elsewhere.[31–35]

Results and Discussion

Crystal Structure of FPP4C and PP4C. ***Amino Twist Angle and Ring Coplanarity.*** The crystal structures of FPP4C and PP4C[36,37] are depicted in Figure 1. As to be expected from the presence of the bridging CH_2 group between the pyrrole and benzonitrile moieties, FPP4C is planar (Figure 1b), with an amino/phenyl twist angle θ of 1.0° (Table 1). With the flexible PP4C, however, an angle θ of 24° is found (Figure 1d and Table 1). This amino twist angle of PP4C is considerably larger than that (5.7°) of crystalline *N*-phenylpyrrole (PP), Table 1.[20] The calculated[37] angle θ = 30.9° of PP4C is somewhat larger than the experimental θ, whereas for PP, much larger twist angles (42.7 and 39.4°) than those in the crystal have recently been calculated.[27,28,38] For FPP4C and PP4C, the experimental pyramidal angle φ of the pyrrole nitrogen is close to zero (Table 1), similar to PP,[20] in accordance with the calculations.[27,28,37]

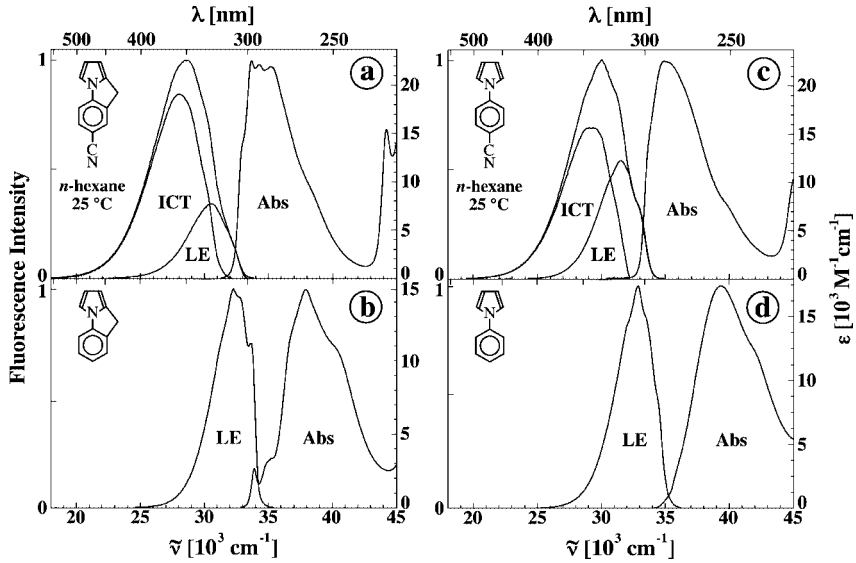

Figure 2. Absorption (Abs) and fluorescence spectra of (a) 4-cyanofluorazene (FPP4C), (b) fluorazene (FPP), (c) 4-cyano-*N*-phenylpyrrole (PP4C), and (d) *N*-phenylpyrrole (PP) in *n*-hexane at 25 °C. The overall fluorescence spectrum of FPP4C in (a) and that of PP4C in (c) is separated into the contributions from the locally excited (LE) and intramolecular charge-transfer (ICT) states. This separation is carried out employing the spectrally shifted LE band of FPP (b) as a model for the LE emission of FPP4C and with the spectrally shifted LE emission band of PP (d) as the LE model for PP4C, with the assumption that the high-energy part of the total fluorescence spectrum only consists of LE emission.

The pyrrole and phenyl rings in the crystalline FPP4C are effectively coplanar.[39] The anisotropic displacement of the methylene carbon C(12) is comparable to that of the other atoms. In the five-membered ring C(1)N(7)C(11)C(12)C(2), the atoms have a mean deviation from planarity of 0.06 pm, but a much larger value of 0.77 pm is found for C(12). The plane through C(1)N(7)C(11)C(2) has a mean distance of 0.4 pm to the atoms, again with the largest deviation of 2.13 pm for C(12). The same conclusion on ring coplanarity is reached by FPP computations.[27,28] The out-of-plane position of C(12) is also seen from the dihedral angles, C(12)C(2)C(1)N(7) = 1.6° and C(12)C(11)N(7)C(1) = 0°.

Pyrrole/Phenyl Bond C(1)−N(7). The experimental (crystal) bond length C(1)−N(7) between the pyrrole and phenyl rings increases in the series FPP4C (139.9 pm), PP4C (140.7 pm), PP (142.3 pm). The calculated bond length of PP4C is the same (141.0 pm)[37,39] as the experimental result, whereas recent computations for PP find a somewhat smaller distance (141.3 and 141.5 pm)[27,28,38] than that obtained[20] from the crystal (142.3 pm); see Table 1.

Pyrrole Ring. The experimental C(9)−C(10) bond length of the rigidified FPP4C (142.3 pm) is clearly larger than that for PP4C (140.8[36] and 141.1 pm[37]) and PP (141.2 pm). The bond C(10)−C(11) of FPP4C (135.9 pm), in contrast, is considerably shorter than that for PP4C (137.0 pm)[36] but similar to that of PP (136.2 pm). The bonds C(8)−C(9), N(7)−C(8), and N(7)−C(11) of FPP4C have lengths comparable to those of PP4C and PP (Table 1). The calculated[37] pyrrole bond lengths of PP4C are all longer than the crystal data,[36] from +2.2 pm for C(9)−C(10) to +0.6 pm for C(8)−C(9) and C(10)−C(11).

Phenyl Ring. The bonds C(1)−C(6) and C(2)−C(3) are shorter for FPP4C than for those PP4C, by amounts of 1.0 and 0.4 pm. The other phenyl bonds of FPP4C are longer than those of PP4C, especially C(3)−C(4) and C(5)−C(6), with increases of 1.0 and 0.8 pm versus PP4C. The same trend is found for FPP4C versus PP (Table 1). The calculated[37] bond lengths of PP4C are longer than the experimental[36] values, from +2.5 pm (C(5)−C(6)) to + 0.6 pm (C(2)−C(3)), except for C(3)−C(4) with −0.5 pm.

Cyano Group. The cyano bond length C(13)−N(14) of FPP4C at 115.0 pm is similar to that of PP4C (114.7 pm).[36] A much shorter experimental C−N bond is reported for PP4C (111.6 pm),[37] whereas 116.5 pm is computed, considerably longer than that experimentally determined for most cyano groups.[1,2] The phenyl−CN bond C(4)−C(13) in the crystal is longer for FPP4C (144.1 pm) than for PP4C[36] (143.2 pm). A C(4)−C(13) bond of 144.6 pm is reported for PP4C, to be compared with a calculated length of 143.5 pm.[37]

Quinoidality. Reduced Pyrrole/Phenyl Electronic Coupling. The quinoidality (C(5) − C(6))/(C(4) − C(5)) in the phenyl rings of FPP4C (0.9950), PP4C (0.9921 and 0.9993),[36,37] and PP (1.001)[20] is close to unity, that is, there is only a small bond length alternation in the phenyl ring. In the computations on PP4C, FPP, and PP, the quinoidality equals 1.0 (Table 1). This negligible bond length alternation is attributed to the relatively long phenyl−pyrrole bond C(1)−N(7), see above, which minimizes the electronic coupling between the pyrrole and phenyl rings. With the 4-aminobenzonitriles, the quinoidality is more pronounced because of the shorter amino−phenyl bond, 0.9793 (4-aminobenzonitrole (ABN), 137.0 pm), and 0.9870 (DMABN, 136.5 pm).[1]For MMD, with a strongly twisted amino group (θ = 59°) and a consequently lengthened amino−phenyl bond (141.4 pm), the phenyl bond length alternation has also become very small (quinoidality: 0.9964).[1] For comparison, in strongly quinoidal molecules, (C(5)−C(6))/(C(4)−C(5)) is 0.9032 (*p*-benzoquinone)[40] and 0.9518 (*p*-benzoquinodimethane).[41]

Twist Angle of PP4C from Comparison with Planarized FPP4C. Absorption Coefficient. The twist angle θ between the pyrrole and benzonitrile moieties of PP4C in the ground state can be determined from the absorption coefficient ε^{max} as compared with that (ε(ref)) of its planarized counterpart FPP4C as the reference compound with zero twist angle (Table 1). This approach, based on eq 1, has been used to estimate θ for nonplanar 4-aminobenzonitriles, 1-aminonaphthalenes and *N*-phenylpyrroles in solution.[10,15,22,42–44]

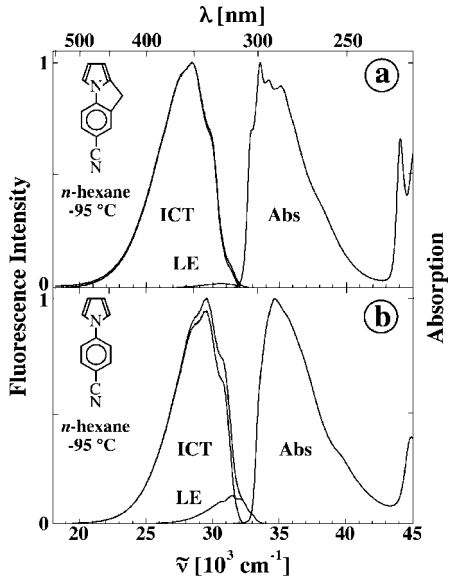

Figure 3. Absorption (Abs) and fluorescence spectra of (a) 4-cyanofluorazene (FPP4C) and (b) 4-cyano-*N*-phenylpyrrole (PP4C) in *n*-hexane at −95 °C. For the determination of Φ′(ICT)/Φ(LE) for FPP4C and PP4C, see Table 2; the ICT emission band is subtracted from the overall fluorescence spectrum, employing the procedure followed in Figure 2a and c.

$$\varepsilon^{max}/\varepsilon(\mathrm{ref}) = \cos^2\theta \qquad (1)$$

From the finding that the ε^{max} in *n*-hexane at 25 °C have similar values for PP4C (22 550 M^{-1} cm^{-1}) and FPP4C (22 600 M^{-1} cm^{-1}), it follows that PP4C in solution is planar in the ground state. The ε^{max} data in MeCN (24 000 vs 23 820 M^{-1} cm^{-1}) lead to the same conclusion; see Table 2. This result shows that the pyrrole/phenyl twist angles θ derived from the X-ray crystal analysis and computations (Table 1) do not necessarily also apply to solution. It has been noted previously for PP that θ has a wide and shallow distribution function due to a relatively small phenyl/pyrrole rotational barrier.[45–47]

Absorption and Fluorescence Spectra of FPP4C and FPP in *n*-Hexane at 25 °C. $\Delta E(S_1,S_2)$. The absorption spectrum of FPP4C in *n*-hexane at 25 °C consists of a structured band with exctinction coefficient ε^{max} = 22 600 M^{-1} cm^{-1} for the maximum at 33 660 cm^{-1} and a shoulder at around 33 000 cm^{-1} with ε = 13 500 M^{-1} cm^{-1} (Figure 2a). For FPP (Figure 2b), a clearly separated relatively weak peak at 33 900 cm^{-1} (ε^{max} = 2640 M^{-1} cm^{-1}) appears on the low-energy edge of the main absorption maximum at 37 900 cm^{-1} (ε^{max} = 14 860 M^{-1} cm^{-1}), with an energy separation of 4000 cm^{-1} between the two peaks in the spectrum. In analogy with the analysis of the absorption spectrum of *N*-phenylpyrrole (PP),[20] the two bands in the spectra of FPP4C and FPP are attributed to the two lowest excited singlet states S_1 and S_2, with a much smaller energy gap $\Delta E(S_1,S_2)$ for FPP4C (1260 cm^{-1}) than in the case of FPP (4000 cm^{-1}) and PP[20] (3900 cm^{-1}); see Figure 2 and Table 2.

In accordance with this small gap,[11–14] the most important contribution to the fluorescence spectrum of FPP4C in *n*-hexane at 25 °C is that of the ICT state (Figure 2a), with an ICT/LE fluorescence quantum yield ratio Φ′(ICT)/Φ(LE) of 3.3 (Table 2). For FPP[26] and PP[20,24,45,46] under these conditions, only a LE emission is observed.

Fluorescence and Absorption Spectra of PP4C and PP in *n*-Hexane at 25 °C. The red shift of the absorption spectrum of PP4C in *n*-hexane at 25 °C relative to that of PP (Figure 2c and d) is similar to that observed for the pair FPP4C/FPP (Figure 2a,b). Likewise, the fluorescence spectrum of PP4C consists of a dual emission (ICT + LE), whereas for PP, only a LE fluorescence is found. The Φ′(ICT)/Φ(LE) ratio of PP4C at 1.5 is somewhat smaller than that for FPP4C (3.3, Table 2), which indicates that the LE → ICT reaction of this molecule is more strongly shifted toward the ICT state.

SCHEME 1

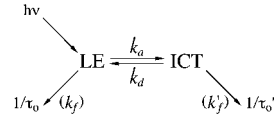

For systems with two kinetically interconverting states, such as LE and ICT in Scheme 1, the ratio Φ′(ICT)/Φ(LE) can be expressed by the following equations[10,13,20,31]

$$\Phi'(\mathrm{ICT})/\Phi(\mathrm{LE}) = k'_f(\mathrm{ICT})/k_f(\mathrm{LE})\{k_a/(k_d + 1/\tau'_o(\mathrm{ICT}))\} \qquad (2)$$

$$\Phi'(\mathrm{ICT})/\Phi(\mathrm{LE}) = k'_f(\mathrm{ICT})/k_f(\mathrm{LE})(k_a/k_d) \qquad (2a)$$

when $k_d \gg 1/\tau'_o(\mathrm{ICT})$ [definition of the high-temperature limit (HTL) (small ICT reaction enthalpy difference $-\Delta H$)].

$$\Phi'(\mathrm{ICT})/\Phi(\mathrm{LE}) = k'_f(\mathrm{ICT})/k_f(\mathrm{LE})(k_a\tau'_o(\mathrm{ICT})) \qquad (2b)$$

when $k_d \ll 1/\tau'_o(\mathrm{ICT})$ [definition of the low-temperature limit (LTL) (large $-\Delta H$)].

In eq 2 and Scheme 1, k_a and k_d are the rate constants of the forward and backward ICT reactions, τ_o(LE) and τ'_o(ICT) are the fluorescence lifetimes, and k_f(LE) and k'_f(ICT) are the radiative rate constants.

FPP4C and PP4C in *n*-Hexane at −95 °C. ICT Reaction Enthalpy Difference ΔH. For FPP4C in *n*-hexane at −95 °C (Figure 3a), Φ′(ICT)/Φ(LE) = 68, much larger than that at 25 °C (3.3, Figure 2a and Table 2). From a linear plot of ln(Φ′(ICT)/Φ(LE)) versus 1000/*T*, a ΔH of −11 kJ/mol is determined (eq 2a and Table 2). This means that FPP4C in *n*-hexane is in the high-temperature limit (HTL, with $k_d \gg 1/\tau'_o$(ICT), eq 2a), valid for ICT systems with a relatively small $-\Delta H$.[13,20,31]

The fluorescence spectrum of PP4C in *n*-hexane at −95 °C (Figure 3b) is similar to that of FPP4C (Figure 3a) under these conditions. The absorption spectrum of PP4C is less structured than that in the case of FPP4C, not unusual for a flexible molecule as compared with a rigidified derivative, such as for the couple biphenyl and fluorene in alkane solvents.[48,49] The same observation is made for PP and FPP; see Figure 2b and d.[26] The Φ′(ICT)/Φ(LE) ratio for PP4C in *n*-hexane at −95 °C is equal to 11, also larger than that (1.5) at 25 °C, see Figure 2c and Table 2, indicating that PP4C in *n*-hexane below 25 °C is in the HTL limit (eq 2a), similar to the condition (small $-\Delta H$) found for FPP4C, as discussed above. For PP4C in *n*-hexane, ΔH = −7 kJ/mol (Table 2), again obtained from a plot of ln(Φ′(ICT)/Φ(LE)) versus 1000/*T*. The energy *E*(FC,ICT), relative to the equilibrated S_0 of the Franck−Condon ground state populated by the ICT fluorescence can be determined via eq 3, employing the data from Table 2, 41 kJ/mol for FPP4C and 40 kJ/mol for PP4C. The large magnitude of *E*(FC,ICT) means that these FC states are not thermally accessible from S_0, ruling out a competitive direct ICT excitation bypassing LE, as will be discussed later.

$$E(\mathrm{FC,ICT}) = E(S_1) + \Delta H - \tilde{\nu}^{max}(\mathrm{ICT}) \qquad (3)$$

Structured ICT Fluorescence Bands of FPP4C and PP4C in *n*-Hexane. The ICT fluorescence bands of FPP4C and PP4C in *n*-hexane at −95 °C are structured (Figure 3). An indication of the presence of such a structure can already be seen for

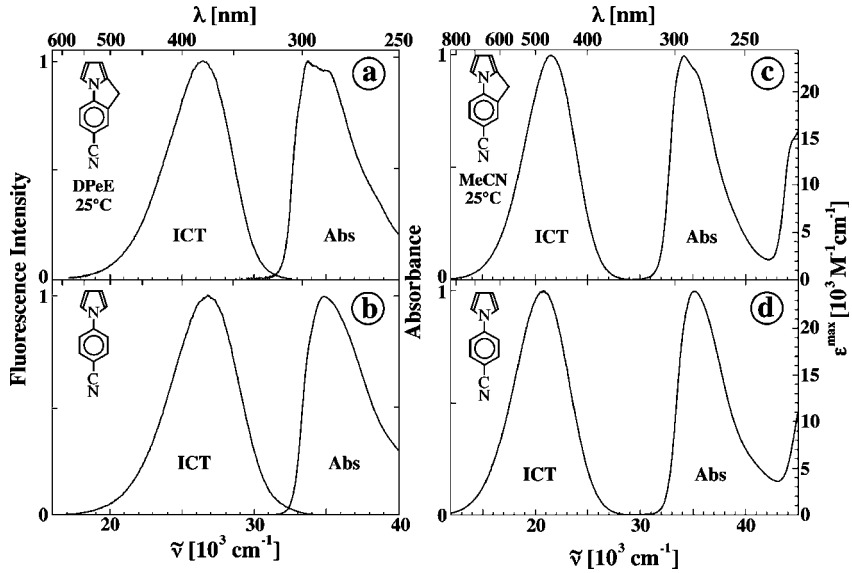

Figure 4. Absorption (Abs) and fluorescence spectra at 25 °C. (a) 4-Cyanofluorazene (FPP4C) and (b) 4-cyano-*N*-phenylpyrrole (PP4C) in di-*n*-pentyl ether (DPeE). (c) FPP4C and (d) PP4C in MeCN. The fluorescence spectra in both solvents consist of a single structureless intramolecular charge-transfer (ICT) band.

FPP4C and PP4C[24] at 25 °C in this solvent (Figure 2a and c). A structured ICT fluorescence has not previously been reported for other D/A molecules (see below). In solvents clearly more polar than *n*-hexane ($\varepsilon^{25} = 1.88$), such as DEE ($\varepsilon^{25} = 4.24$), THF ($\varepsilon^{25} = 7.39$), and MeCN ($\varepsilon^{25} = 36.7$), the ICT fluorescence band of PP4C is broad and structureless.[22,24,25,45,46,50]

Single ICT Emission Bands without Structure. FPP4C and PP4C in Di-*n*-pentyl Ether and Acetonitrile. In di-*n*-pentyl ether (DPeE, $\varepsilon^{25} = 2.86$), a solvent only slightly more polar than *n*-hexane, the fluorescence spectra of FPP4C and PP4C at 25 °C consist of a single ICT emission band, without any evidence for the presence of a LE emission (Figure 4a and b). Different from the spectra in *n*-hexane (Figures 2a and c and 3), the ICT band does not show any vibrational structure in DPeE nor at lower temperatures; see the spectra at −60 °C in the Supporting Information (Figure S1). The ICT emission band of FPP4C and PP4C[24,25,45,46,50] remains without structure in all solvents other than alkanes and pFMCH, from the dialkyl ethers to MeCN (Figure 4) and methanol. The same is observed for 3-cyano-*N*-phenylpyrrole (PP3C) in DEE and MeCN (no ICT in *n*-hexane)[24,25] and similarly for FPP in MeCN[26] and PP[19,20,24] in THF and alkyl cyanides. The last two molecules do not undergo an ICT reaction in *n*-hexane and DEE.[26] It is therefore concluded that with FPP4C and PP4C in *n*-hexane (structured ICT emission), only a small structural difference exists between the ICT and the corresponding ground state, whereas in MeCN (no structure), the large μ_e(ICT) leads to a solvent-induced shift of the ICT potential energy surface relative to S_0.

Structureless ICT Fluorescence Bands of 4-Aminobenzonitriles in All Media. The structureless ICT fluorescence bands reported above for the *N*-phenylpyrroles in solvents other than alkanes are similar to the ICT bands observed with the dual fluorescent 4-aminobenzonitriles, such as DMABN,[9,11–13,31,33,51] 6-cyanobenzoquinuclidine (CBQ),[9,11] a series of 2,3,5,6-tetrafluoro-4-aminobenzonitriles XABN4F,[33,51] and NTC6.[10,15] With the 4-aminobenzonitriles, however, the ICT fluorescence band is also structureless in *n*-hexane, different from FPP4C and PP4C. Examples of molecules with such broad bands in *n*-hexane are CBQ,[11] DIABN,[10] 4-(*tert*-butylmethylamino)benzonitrile,[10]4-(di-*tert*-butylamino)benzonitrile (DTABN),[52] 3-(di-*tert*-butylamino)benzonitrile (mDTABN),[52] NTC6,[10,15] and the XABN4Fs, with a dimethylamino,[33,51] diethylamino,[33] azetidinyl,[33] methylamino,[33] and amino[33] substituent. Even in the vapor,[53] as well as in the solid[4,5] and molten[5] crystalline phases of DIABN, structure does not appear in the ICT fluorescence band.

Structured Fluorescence Spectrum of DCS in *n*-Hexane. A structured fluorescence spectrum in *n*-hexane and the simultaneous complete absence of structure in all other aprotic solvents, from di-*n*-hexylether ($\varepsilon^{25} = 2.75$) to MeCN ($\varepsilon^{25} = 36.7$), have also been observed in the case of 4-dimethylamino-4′-cyanostilbene (DCS), an ICT compound with a large dipole moment (21 D).[54] This loss of vibrational structure with DCS and related substances may be caused by the onset of specific solvation.[54,55] Different from FPP4C and PP4C, the presence of a LE precursor could not be detected for DCS, as established by experiments with picosecond and femtosecond time resolution.[54–57]

Dependence of the Excitation Wavelength of the Fluorescence and Excitation Spectra of FPP4C and PP4C in *n*-Hexane at 25 °C. The observation that the spectral band at the high-energy side in the fluorescence spectra of FPP4C and PP4C in *n*-hexane becomes smaller upon cooling (Figures 2a and c and 3) is an indication that this emission comes from the LE state and not from an impurity. To further establish that it is indeed a LE emission, fluorescence and excitation spectra were measured at wavelengths spanning the absorption and emission spectra (Figure 5). These experiments were considered to be important; as in the femtosecond excited-state absorption spectra with FPP4C and PP4C in *n*-hexane (presented below), clear evidence for a time development was missing. From the absence of an excitation wavelength dependence of the fluorescence spectra for FPP4C and PP4C, it is concluded that both molecules indeed undergo an ICT reaction in *n*-hexane and that dual fluorescence (LE and ICT) appears in this solvent (Figures 2 and 3). Dual emission has also been found with PP4C in cryogenic matrices.[58] The independence of the fluorescence spectra of FPP4C and PP4C in *n*-hexane on excitation wavelength (Figure 5) indicates that the ICT reaction of these molecules starts from the S_1(LE) state as the precursor, following an adiabatic reaction pathway. The same conclusion has been made for the ICT reaction of DMABN in THF and of *N*,*N*-di-

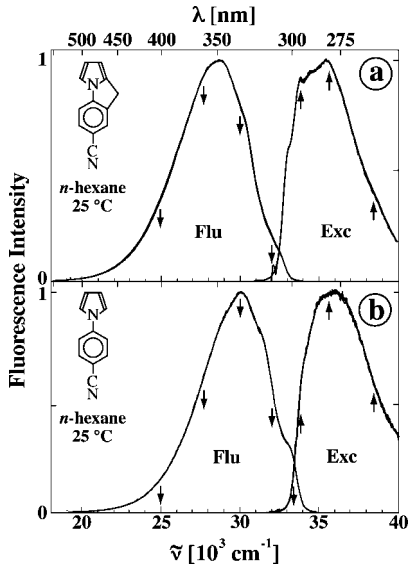

Figure 5. (a) Fluorescence (Flu) and excitation (Exc) spectra of 4-cyanofluorazene (FPP4C) in *n*-hexane at 25 °C. For the fluorescence spectra, the excitation wavelengths are 260, 280, and 295 nm. For the excitation spectra, the emission wavelengths are 312, 330, 360, and 400 nm. (b) Fluorescence and excitation spectra of 4-cyano-*N*-phenylpyrrole (PP4C) in *n*-hexane at 25 °C. For fluorescence spectra, the excitation wavelengths are 295, 280, and 260 nm. For the excitation spectra, the emission wavelengths are 300, 312, 330, 360, and 400 nm.

n-propyl-4-(trifluoromethyl)aniline (DPrCF3) in MeCN, likewise based on the absence of excitation wavelength dependence for the dual fluorescence spectra.[59]

Solvatochromic Measurements. ICT Dipole Moment μ_e(ICT) of FPP4C. For the determination of the dipole moment μ_e(ICT) of FPP4C, the maximum $\tilde{\nu}^{max}$(ICT) of the fluorescence band was measured in a series of solvents, from the nonpolar perfluoromethylcyclohexane (pFMCH, $\varepsilon^{25} = 1.82$) to the strongly polar MeCN ($\varepsilon^{25} = 36.7$); see Table 3.

The ICT dipole moment can be obtained from the slope of the plot of $\tilde{\nu}^{max}$(ICT) versus the solvent polarity parameter $f(\varepsilon) - {}^1/_2 f(n^2)$, eqs 4–6,[24,54,60–62] resulting in μ_e(ICT) = 14.8 D (Figure 6a). By plotting the $\tilde{\nu}^{max}$(ICT) of FPP4C against those of DIABN (18 D)[63] in the same solvent series (Figure 6b), a comparable μ_e(ICT) = 15.7 D is calculated; see Table 4. With this procedure, the scatter in the data points is generally reduced by mutually compensating for the specific solute/solvent interactions.[10,33,54,63] For PP4C, similar ICT dipole moments were reported, 16.3 D relative to DMABN (17 D)[64,65] and 16.1 D versus $f(\varepsilon) - {}^1/_2 f(n^2)$.[24] Other literature values for μ_e(ICT) of PP4C are 22.4 D[22] and 14.8 D.[25]

$$\tilde{\nu}^{max}(\text{flu}) = -\frac{1}{2hc\rho^3}\mu_e(\mu_e - \mu_g)g(\varepsilon, n) + \text{const} \quad (4)$$

$$f(\varepsilon) = \frac{(\varepsilon - 1)}{(2\varepsilon + 1)} \quad (5)$$

$$f(n^2) = \frac{(n^2 - 1)}{(2n^2 + 1)} \quad (6)$$

In eqs 4–6, μ_g and μ_e are the ground and excited-state dipole moments, ε is the dielectric constant, n the refractive index, ρ the Onsager radius of the solute, and $g(\varepsilon,n) = f(\varepsilon) - {}^1/_2 f(n^2)$.[10,24,33]

Picosecond Fluorescence Decays of FPP4C in *n*-Hexane at 25 °C. The picosecond fluorescence decay i_f (eqs 7 and 8) of FPP4C in *n*-hexane at 311 nm, a wavelength where the emission comes predominantly from the LE state (Figure 2a), is a double exponential with a main decay time τ_1 of 14.3 ns and a minor short decay time τ_2 of 7 ps (Figure 7a). Contrary to other systems undergoing a fast ICT reaction, such as NTC6 in *n*-hexane at 25 and −95 °C,[15] a growing-in (negative amplitude A_{22}, eq 8) is not observed for the ICT fluorescence decay. This already shows that the time τ_2 of 7 ps does not represent the ICT reaction time of FPP4C in this solvent. From femtosecond excited-state absorption (ESA) measurements, to be presented in a later section, it indeed follows that the LE → ICT reaction of FPP4C in *n*-hexane takes place in the subpicosecond time range, too fast for our picosecond SPC experiments.

$$i_f(\text{LE}) = A_{11}\exp(-t/\tau_1) + A_{12}\exp(-t/\tau_2) \quad (7)$$

$$i_f(\text{ICT}) = A_{21}\exp(-t/\tau_1) + A_{22}\exp(-t/\tau_2) \quad (8)$$

Picosecond Fluorescence Decays of PP4C in *n*-Hexane at 25 °C. The picosecond fluorescence decays of PP4C were measured in *n*-hexane at 25 °C. The decay at 305 nm, in the spectral range of the LE emission (Figure 2c), is a double exponential, with a main long decay time τ_1 of 3.13 ns and a small but not negligible contribution from $\tau_2 = 6$ ps. The decay at the ICT emission wavelength of 390 nm can also be fitted as a double exponential with 6 ps and 3.13 ns (global analysis), with a growing-in of the short component ($A_{22} = -0.15$, eq 8). Similar to the situation for FPP4C in *n*-hexane described above, the time τ_2 of 6 ps is much longer than the ICT reaction time determined from ESA experiments.

Picosecond Fluorescence Decays of FPP4C and PP4C in MeCN at 25 °C. The fluorescence decays at the ICT emission maxima of FPP4C and PP4C in MeCN at −45 °C (Figure 8) can be fitted as single exponentials, with decay times τ_1 of 39.2 and 16.7 ns, respectively. The fluorescence spectra of FPP4C and PP4C in MeCN at 25 °C consist of a single broad ICT emission band (Figure 4c and d), without any indication of the presence of a LE fluorescence. This is the case over the entire investigated temperature range from 75 to −45 °C. It is hence concluded that the ICT reaction with FPP4C and PP4C in MeCN is faster than the time resolution (~3 ps) of the picosecond fluorescence decays, as also seen from the femtosecond ESA experiment (see below).

The picosecond fluorescence decays of FPP4C and PP4C in other solvents more polar than alkanes, such as DEE, DPeE, DBE, THF, and EtCN, can be fitted with a single exponential when measured at the emission maximum, similar to Figure 8. At other emission wavelengths, the fluorescence decays require an additional exponential for an acceptable fitting. This short second decay time τ_2, in the range between 3 and 10 ps, is attributed to a dynamic Stokes shift[43,66,67] because the ICT reaction takes place in the subpicosecond time range, as mentioned above. A dynamic Stokes shift is usually brought about by a change in molecular structure during the excited lifetime. An example is the planarization of the amino group of 1-(dimethylamino)naphthalene.[43,66,67] The apparent decay times of these multiexponential decays do not have a direct physical meaning in terms of reaction rate constants, but time-resolved fluorescence spectra can be constructed from the decays measured over the entire fluorescence spectrum, such as for NTC6.[15]

Fluorescence Decays of FPP4C and PP4C as a Function of Temperature. The temperature dependence of the longest (nanosecond) decay time τ_1 (see Figures 7 and 8) of FPP4C in *n*-hexane, DEE, and MeCN, as well as that of PP4C in *n*-hexane and MeCN, is presented in Figure 9. It is seen that τ_1 becomes

TABLE 3: ICT Fluorescence Maxima $\tilde{\nu}^{max}$(ICT) in 1000 cm^{-1} of 4-Cyanofluorazene (FPP4C), 4-Cyano-*N*-phenylpyrrole (PP4C), and 4-(Diisopropylamino)benzonitrile (DIABN) at 25 °C in a Series of Solvents Spanning the Polarity Scale of $f(\varepsilon) - {}^1/_2 f(n^2)$ (Eqs 5 and 6)

solvent	ε	n	$f(\varepsilon)$	$f(n^2)$	$f(\varepsilon) - 1/2f(n^2)$	FPP4C [1000 cm^{-1}]	PP4C[a] [1000 cm^{-1}]	DIABN[b] [1000 cm^{-1}]
pFMCH[c] (1)	1.82	1.279	0.177	0.149	0.102	28.47	(29.60)	26.08
n-pentane (2)	1.83	1.355	0.179	0.179	0.089	28.02		25.76
n-hexane (3)	1.88	1.372	0.185	0.185	0.092	28.00	29.03	25.72
di(*n*-pentyl) ether (4)	2.86	1.412	0.277	0.199	0.177	26.44	26.83	24.37
di(*n*-butyl) ether (5)	3.05	1.397	0.289	0.194	0.192	26.27	26.64	24.30
di(*n*-propyl) ether (6)	3.26	1.379	0.301	0.188	0.207	26.00	26.24	24.09
diethyl ether (7)	4.24	1.350	0.342	0.177	0.253	25.35	25.17	23.52
tetrahydrofuran (8)	7.39	1.405	0.405	0.197	0.307	23.60	23.30	22.38
ethyl acetate (9)	5.99	1.370	0.384	0.184	0.292	23.54	23.15	22.26
n-butyl cyanide (10)	19.8	1.395	0.463	0.193	0.366	22.66		21.30
n-propyl cyanide (11)	24.2	1.382	0.470	0.189	0.375	22.33	21.60	21.09
ethyl cyanide (12)	29.2	1.363	0.470	0.182	0.384	22.02	21.32	20.87
acetonitrile (13)	36.7	1.342	0.480	0.174	0.393	21.52	20.75	20.49

[a] Data from ref 24 except for *n*-hexane and acetonitrile. [b] Data from ref 33. [c] Perfluoromethylcyclohexane.

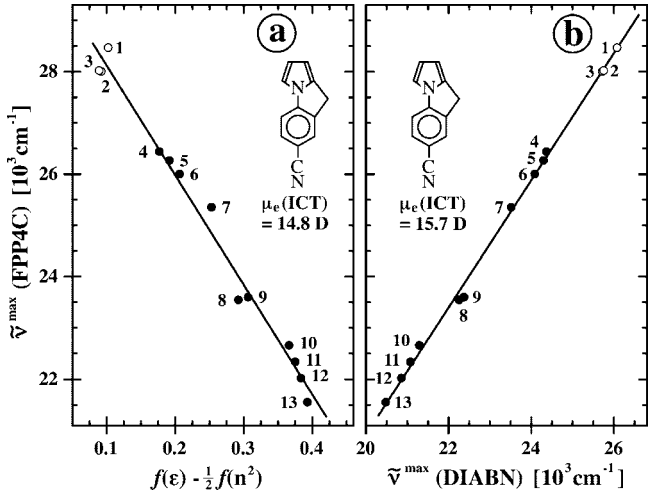

Figure 6. Solvatchromic plots of the ICT fluorescence maxima $\tilde{\nu}^{max}$(ICT) of 4-cyanofluorazene (FPP4C) versus (a) the solvent polarity parameter $f(\varepsilon) - {}^1/_2 f(n^2)$ and (b) $\tilde{\nu}^{max}$(ICT) of 4-(diisopropylamino)benzonitrile (DIABN); see eqs 4–6. For the $\tilde{\nu}^{max}$(flu) and the numbering of the solvents, see Table 3. From the slopes of the plots, the ICT dipole moment μ_e(ICT) of FPP4C is calculated, 14.8 D for (a) and 15.7 D for (b); see eq 4 and the text. Points 1−3 (open circles) are not included in the analysis, as in these solvents dual fluorescence (LE + ICT) is observed.

TABLE 4: Data from the Solvatochromic Analysis of the ICT Fluorescence Maxima $\tilde{\nu}^{max}$(ICT) of 4-Cyanofluorazene (FPP4C)

	ρ [Å][a]	μ_g [D][b]	slope	μ_e(ICT) [D][c]
FPP4C (eq 4)	4.33	3.18[d]	−21 400 ± 800[e]	14.8 ± 0.2
FPP4C (vs DIABN)[f]	4.33 (4.68)	3.18[d] (6.8)	1.24 ± 0.03[g]	15.7 ± 0.2 (18)

[a] Onsager radius (eq 4), determined from a density equal to 0.78, based on DMABN (ref 24). [b] Ground-state dipole moment. [c] ICT dipole moment (eq 4). [d] Calculated by AM1; result scaled by μ_g(DMABN) = 6.6 D (ref 65). [e] From a plot of $\tilde{\nu}^{max}$(FPP4C) versus $g(\varepsilon,n)$, eqs 4–6; see Figure 6a. [f] From DIABN, ρ = 4.68 Å, μ_g = 6.8 D, μ_e(ICT) = 18 D, from refs 24 and 33. [g] From a plot of $\tilde{\nu}^{max}$(ICT) of FPP4C versus $\tilde{\nu}^{max}$(ICT) of DIABN (Figure 6b).

longer with increasing solvent polarity, from (at 25 °C) 12.8 ns in *n*-hexane to 30 ns in MeCN for FPP4C and from 3.1 to 13.6 ns in these solvents for PP4C.

Radiative Rate Constants k'_f(ICT) for FPP4C and PP4C. The radiative rate constants k'_f(ICT) of FPP4C were determined at 25 °C as a function of solvent polarity by employing eq 9. The results for this rigidified molecule are compared with those of its flexible counterpart PP4C (Table 5). Equation 9 is only valid when the fluorescence spectrum predominantly consists of an ICT emission, that is, when Φ(LE) is effectively zero.[20,68] When this condition does not hold, the more complex general expression eq 10 should be employed for k'_f(ICT). In such a case, the overall fluorescence spectra have to be separated into the LE and ICT contributions, and data for k_a, k_d, τ'_o(ICT) and τ_o(LE) (Scheme 1) are required. These last data can only be obtained from a full kinetic analysis of the LE fluorescence decays, which could not be made for FPP4C and PP4C in *n*-hexane, as discussed above.[13,15,20,31]

$$k'_f(\mathrm{ICT}) = \Phi'(\mathrm{ICT})/\tau_o(\mathrm{ICT}) \quad (9)$$

$$k'_f(\mathrm{ICT}) = \Phi'(\mathrm{ICT})\{1/\tau'_o(\mathrm{ICT}) + 1/\tau_o(\mathrm{LE})[(k_d + 1/\tau'_o(\mathrm{ICT}))/k_a]\}$$

$$= \Phi'(\mathrm{ICT})\{1/\tau'_o(\mathrm{ICT}) + F\} \quad (10)$$

where $F = 1/\tau_o(\mathrm{LE})\ [(k_d + 1/\tau'_o(\mathrm{ICT}))/k_a]$.

For FPP4C and PP4C, similar values are obtained for k'_f(ICT) (Table 5), showing again[14] that the radiative rate constant is not small due to the presence of a twisted ICT state but is caused by the differences in electronic structure between the ICT and S_0 states.[14,69] It should be noted that the TICT configuration reported for PP4C in the literature was based on its assumedly small radiative rate constant k'_f(ICT),[25] shown here to be comparable to that of the planar FPP4C (Table 5).

The k'_f(ICT) data are corrected for the influence of the energy of the ICT emission maximum $\tilde{\nu}^{max}$(ICT) and the solvent refractive index n (eq 11).[48,70,71] On the basis of Planck's blackbody radiation law, a dependence of k'_f(ICT) on $(\tilde{\nu}^{max}(\mathrm{ICT}))^3$ and n^3 would be expected, as seen from eq 11, where $|M_f|$ is the ICT transition dipole moment.[48] An equation with n^2 was also introduced,[48,70] as well as one with $n^2/(2n^2 + 1)$ in a treatment[71] with a spherical empty solvent cavity. After dividing k'_f(ICT) of FPP4C and PP4C by $(\tilde{\nu}^{max}\ (\mathrm{ICT}))^3 n^3$ (eq 11), a procedure usually adopted in the literature,[9,72] its solvent polarity dependence has disappeared (Table 5). The same result is found, however, by correcting with n^2 (Table 5). Differentiation between n^3 and n^2 is experimentally difficult because of intrinsic inaccuracies in measuring fluorescence quantum yields

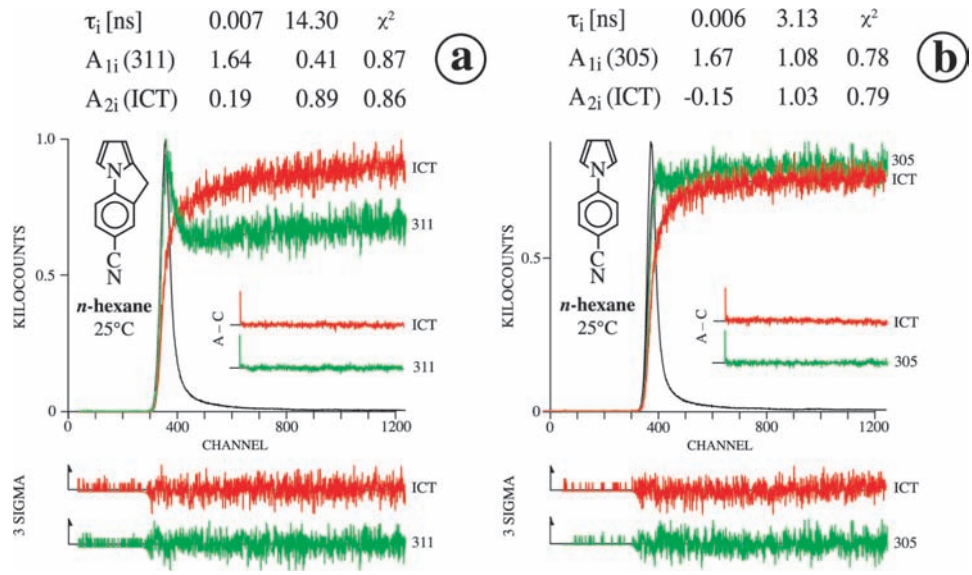

Figure 7. Double exponential fluorescence decays in *n*-hexane at 25 °C. (a) 4-Cyanofluorazene (FPP4C) at 311 and 370 nm (ICT) (Figure 2a). (b) 4-Cyano-*N*-phenylpyrrole (PP4C) at 305 and 390 nm (ICT) (Figure 2b). The decay times τ_2 and τ_1 with the corresponding amplitudes A_{1i}(311) or A_{1i}(305) and A_{2i}(ICT), see eqs 7 and 8, are given in the figure. The shortest decay time is listed first. The weighted deviations sigma, the autocorrelation functions A−C, and the values for χ^2 are also indicated. Excitation wavelength: (a) 272 nm, (b) 276 nm. Time resolution: 0.496 ps/channel with a time window of 1200 effective channels.

and, to a smaller extent, decay times. See, as an illustration, the large variations in the published fluorescence quantum yields for PP4C[22,24,25,46,50] (Table 5).

$$k'_f(\mathrm{ICT}) = |M_f|^2(64\pi^4(\tilde{\nu}^{\max}(\mathrm{ICT}))^3 n^3)/3h \qquad (11)$$

It has previously been reported that k'_f(ICT) likewise does not depend on solvent polarity for MMD and CBQ,[72] which do not show appreciable LE emission next to the ICT fluorescence and for which eq 9 is hence valid.

Transient Absorption Spectra of FPP4C in *n*-Hexane. The transient absorption spectrum of FPP4C in *n*-hexane, shown for six pump−probe delay times between 0.1 and 5.0 ps (Figure 10a), consists of two broad bands with maxima around at 445 and 700 nm. After subtraction of the stimulated emission (SE), the excited-state absorption (ESA) spectra are obtained (Figure 10b). The long-wavelength maximum shifts and decays from 725 nm at a pump−probe delay time of 100 fs to 695 nm at a 5 ps delay, whereas the 445 nm maximum does not undergo such a shift. A growing-in is observed at around 445 nm, and a decay is observed between 640 and 1000 nm. The first band could hence be associated with the ICT and the second with the LE state.

Identification of ESA Bands. The identification of the absorption bands of FPP4C in Figure 10b (spectral window 334−1072 nm) is based on a comparison with the LE and ICT ESA spectra of DMABN in *n*-hexane and MeCN. The LE spectrum of DMABN in *n*-hexane (no ICT) has maxima at 300−320, 445, and 745 nm (Table 6). The ESA spectra in this solvent of FPP and PP, for which ICT likewise does not take place,[20,24,26] also have a similar LE maximum at around 700 nm.[73] In MeCN, the main LE maxima of DMABN are at 320, 355, 440, and 710 nm, whereas those for the ICT absorption occur at 315 and 425 nm.[31] With the planarized DMABN derivative NTC6, the ESA maxima for LE are at 470 and 800 nm in *n*-hexane (0.2 ps delay time), and for ICT, they are at 435 nm and below 334 nm in MeCN (5 ps delay time); see Table 6.[15]

It is hence concluded that the 700 nm band of FPP4C originates from LE, whereas the band at around 445 nm contains contributions from LE and ICT. This identification is verified by the absence of a band at around 700 nm in the ICT ESA spectra of FPP4C and PP4C in MeCN at a pump−probe time delay larger than 1 ps; see below (Figures 12 and 13). As a further support, a LE emission could not be detected in the fluorescence spectra of FPP4C and PP4C in MeCN (Figure 4c and d). The similarity of the ICT states of DMABN and PP4C has previously been inferred from their picosecond IR spectra in MeCN.[23]

Superposition of LE and ICT Spectra. The ESA spectrum of FPP4C in *n*-hexane (Figure 10b) is a superposition of LE (700 nm) and ICT (445 nm) spectra, from a comparison with the LE and ICT ESA spectra of DMABN. Besides the ICT state, also the LE state contributes to the absorption band at around 445 nm. The strong presence of the LE ESA band means that an equilibrium exists between LE and ICT (Scheme 1). This interpretation is supported by the analysis of the temperature dependence of the ratio Φ'(ICT)/Φ(LE) in *n*-hexane, showing that FPP4C is in the HTL limit, associated with a small $-\Delta H$ (11 kJ/mol, Table 2).[13,68]

Time Development of ESA Spectra. In the ESA spectra of FPP4C in *n*-hexane at pump−probe delay times between 100 fs and 5 ps (Figure 10b), the LE absorption band (around 700 nm) is strongly present in addition to the LE + ICT band at 445 nm, and only a minor decay and growing-in is observed. At a delay time of 100 fs, the ESA spectrum is already nearly fully developed. This could mean that the ICT reaction is very fast, at the limit of the experimental time resolution (50 fs). As the fluorescence spectrum of FPP4C in *n*-hexane mainly consists of an ICT emission (Figure 2a), it is obvious, however, that an effective ICT reaction in fact takes place with FPP4C in *n*-hexane. The small time development of the ESA spectra therefore means that an ultrafast equilibrium between LE and ICT is indeed already established at 100 fs after excitation. Further support for this interpretation comes from femtosecond IR measurements with FPP4C and PP4C in *n*-hexane,[74] which show that the frequeny of their cyano vibration (2120 and 2132

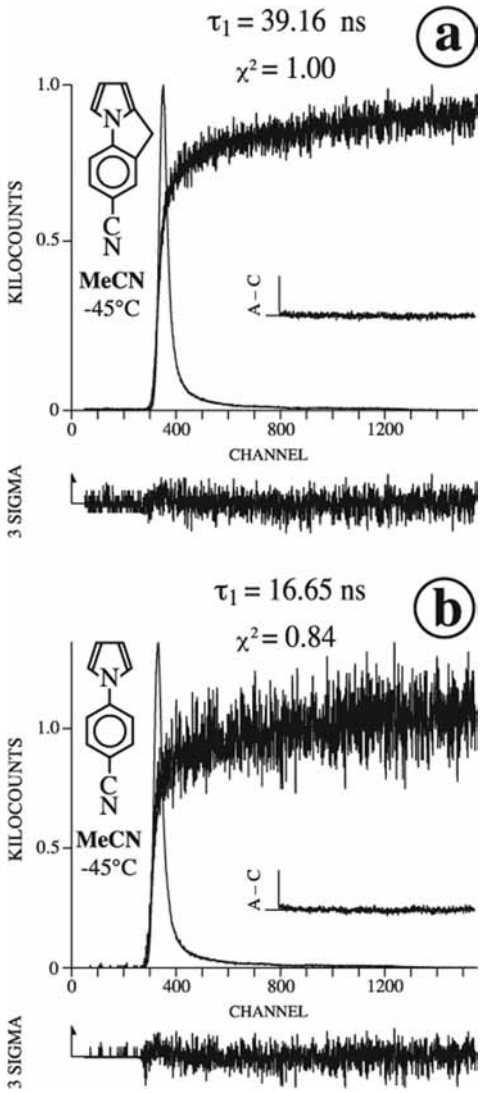

Figure 8. Single exponential ICT fluorescence decays of (a) 4-cyanofluorazene (FPP4C) and (b) 4-cyano-*N*-phenylpyrrole (PP4C) in acetonitrile (MeCN) at −45 °C. The decay time τ_1 is given in the figure. Emission wavelength: (a) 465 nm, (b) 480 nm; compare Figure 5a and b (at 25 °C). Excitation wavelength: 272 nm. Time resolution: 0.496 ps/channel with a time window of 1500 effective channels. See the caption of Figure 7.

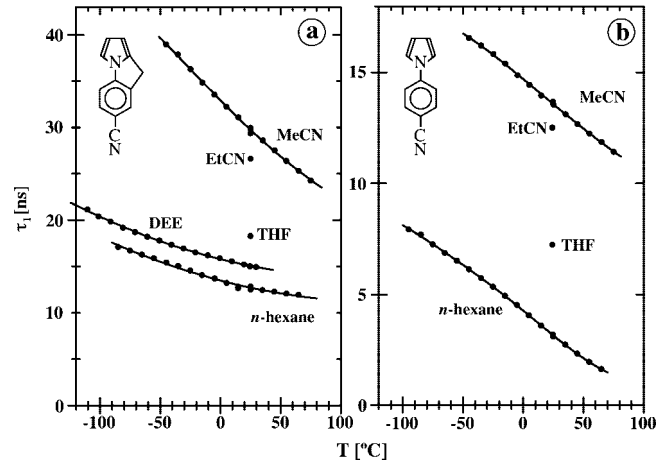

Figure 9. Longest fluorescence decay time τ_1 (cf. Figures 7 and 8) as a function of temperature for (a) 4-cyanofluorazene (FPP4C) and (b) 4-cyano-*N*-phenylpyrrole (PP4C). The data points at 25 °C for tetrahydrofuran (THF) and ethyl cyanide (EtCN) are also indicated (Table 5). Note the different vertical time scale for (a) and (b).

cm^{-1}) is similar to that (2095 cm^{-1}) of the ICT state of DMABN,[75–77] strongly down-shifted from the LE frequency at 2180 cm^{-1}.

From the minor temporal change of the band integral BI(640,900), covering the LE absorption band, a decay time of 650 fs is determined (Figure 10c), which could be related to the LE → ICT reaction time of FPP4C in *n*-hexane (eq 12). The band integral BI(380,470), in the spectral range of the ICT absorption, shows a much longer growing-in of 7 ps, a time which is clearly not the ICT reaction time of FPP4C but is attributed to vibrational cooling, as in the case of the ICT reaction with NTC6 and DMABN.[15,31] A decay time of 7 ps was also found in the picosecond fluorescence decay of FPP4C in *n*-hexane (Figure 7a). Apart from the 650 fs decay, BI(640,900) remains practically constant over the time window of 5 ps (reflected by the offset with amplitude A_0, eq 12), as is to be expected from the decay time of $\tau_1 = 14.3$ ns of the FPP4C fluorescence (Figure 7a). On a larger time scale (110 ps), Figure S2 in Supporting Information, likewise, no change occurs in the ESA spectrum for delay times longer than 5 ps. A global analysis of the LE and ICT decays BI(380,470) and BI(640,980) gives the times of 650 fs and 7 and 70 ps (Figure S2).

$$\Delta\mathrm{OD} = A_{i3}\exp(t/\tau_{i3}) + A_{i2}\exp(t/\tau_{i2}) + A_{i1}\exp(t/\tau_{i1}) + A_0 \quad (12)$$

Under the present circumstances of ultrafast ICT at the limit of the experimental time resolution, the decay times obtained from fitting the decay of ESA band integrals cannot be used for an accurate determination of the rate constants of the LE → ICT reaction (Scheme 1), as discussed above for the fluorescence decay times. A similar situation is encountered in the case of a dynamic (or horizontal) Stokes shift caused by structural and environmetal changes of a molecule/solvent system with a single excited state, as mentioned above.[78,79]

Transient Absorption Spectra of PP4C in *n*-Hexane. The transient absorption spectra of PP4C in *n*-hexane, with pump−probe delay times between 0.2 and 120 ps, are shown in Figure 11a. The ESA spectra, obtained by subtracting the stimulated emission (Figure 11b), consist of two bands at around 410 and 750 nm. The spectra show a similarity with those of FPP4C (Figure 10), and the same identification of the absorption bands is adopted, a LE band (decay) with maxima between 765 (0.2 ps delay) and 730 nm (120 ps delay) and a mixture of ICT and LE for the band with maxima at 380 (growing-in, ICT) and 445 nm (decay, LE). The ESA bands undergo little time development, which means, similar to what was found for FPP4C, that the LE and ICT states of PP4C in *n*-hexane are in rapid equilibrium and are already present to a large extent at 200 fs after excitation. This conclusion is supported by the observation of both LE and ICT emission in the fluorescence spectrum of PP4C in *n*-hexane (Figure 2c). The occurrence of an efficient ICT reaction with PP4C has also been found in a cryogenic argon matrix, having a relatively small effective dielectric constant, even somewhat smaller than that of *n*-hexane.[80]

The minor decay of the band integral BI(650,1000) of PP4C, showing the time development of the LE state, can be fitted with a short decay time of 480 fs and a longer time of 35.4 ps (Figure 11c). The time of 480 fs, interpreted as an indication of the ICT reaction time, also appears from the fitting of the decay of the more complex BI(410,490), covering a superposi-

TABLE 5: Radiative Rate Constants k'_f(ICT) for 4-Cyanofluorazene (FPP4C) and 4-Cyano-*N*-phenylpyrrole (PP4C) at 25 °C, Calculated (Eq 9) from the Fluorescence Quantum Yield Φ'(ICT) and the Lifetime τ'_o(ICT). The Refractive Index *n* of the Solvents and the ICT Emission Maxima $\tilde{\nu}_{max}$ (ICT) are also Listed

		FPP4C					PP4C				
solvent	n_D	k'_f(ICT) [10^7 s^{-1}]	$k'_f(ICT)^{corr,a}$	Φ'(ICT)	τ'_o(ICT) [ns]	$\tilde{\nu}^{max}$(ICT) [1000 cm^{-1}]	k'_f(ICT) [10^7 s^{-1}]	$k'_f(ICT)^{corr,a}$	Φ'(ICT)	τ'_o(ICT) [ns]	$\tilde{\nu}^{max}$(ICT) [1000 cm^{-1}]
DBE[b]	1.404	1.62	3.2 (4.5)	0.24	14.80	26.27	1.19	2.4 (3.3)	0.039	3.29	26.64
DEE[c]	1.361	1.29	3.1 (4.2)	0.20	15.51[d]	25.35	0.89	2.2 (2.9)	0.033	3.72	25.17
THF[d]	1.405	1.04	2.8 (4.0)	0.19	18.30	23.60	0.67	1.8 (2.6)	0.049	7.33	23.30
EtCN[e]	1.364	0.90	3.3 (4.5)	0.24	26.59	22.02	0.54	2.0 (2.7)	0.068	12.50	21.32
MeCN[f]	1.342	0.84	3.5 (4.7)	0.25	29.74	21.52	0.47	1.9 (2.6)	0.064	13.57	20.75

[a] $k'_f(ICT)^{corr} = k'_f(ICT)/(n_D^3(\tilde{\nu}^{max}(ICT))^3)$, [$10^{-25}$ cm^3 s^{-1}]; see eq 11. Number in parentheses: n^2 instead of n^3; see text. [b] Di(*n*-butyl) ether. [c] Diethyl ether. [d] Tetrahydrofuran. [e] Ethyl cyanide. [f] Acetonitrile.

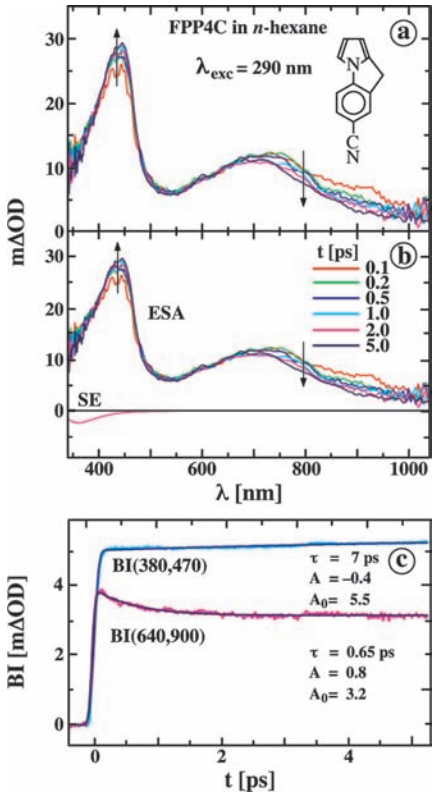

Figure 10. 4-Cyanofluorazene (FPP4C) in *n*-hexane at 290 nm excitation. (a) Transient absorption spectra and (b) excited-state absorption (ESA) spectra after subtraction of the stimulated emission (SE), at pump−probe delay times between 0.1 and 5.0 ps. The SE spectrum (LE and ICT, cf. Figure 2a) is also depicted. In (b), the downward arrow (800 nm) indicates the minor decay of the LE absorption, and the upward arrow (440 nm) shows the small rise of the ICT absorption. (c) The band integral BI(380,470) between 380 and 470 nm in the ESA spectrum has a growing-in time τ of 7 ps, whereas BI(640,900) decays with 650 fs. The amplitude *A* and the offset A_0 are also presented (eq 12). The mΔOD is the optical density/1000.

tion of the ICT and LE absorption bands, which may mask the growing-in (negative amplitude, eq 12) expected for an ICT state. The time $\tau_{i2} = 12$ ps is attributed to vibrational cooling.[15,31] Both absorption bands slowly decay ($\tau_{i1} = 35.4$ ps), in accordance with the long ICT fluorescence decay time τ_1 of 3.13 ns (Figure 7b). With 266 nm excitation, a similar ESA spectrum is obtained for PP4C in *n*-hexane (Figures S3 and S4).

Comparison of ESA and Fluorescence Spectra of FPP4C and PP4C in *n*-Hexane. A comparison of the ESA spectra of FPP4C (Figures 10b and S2) and PP4C (Figure 11b) in *n*-hexane shows that the relative intensity of the longer-wavelength LE band (around 700 nm for FPP4C and 750 nm for PP4C) as compared with that at around 445 nm (LE + ICT) is smaller for FPP4C than that for PP4C. At a pump−probe time delay of 5 ps, for example, the LE/(LE + ICT) intensity ratios are 0.38 for FPP4C and 0.48 for PP4C. At a delay time of 120 ps, the following ratios are obtained: 0.32 (FPP4C, Figure S2) and 0.43 (PP4C, Figure 11b). This means that for FPP4C, the equilibrium between LE and ICT is shifted more into the direction of ICT than that for PP4C, that is, the ICT reaction in *n*-hexane is more efficient with FPP4C than with PP4C. This conclusion is supported by the fluorescence quantum yield ratio Φ'(ICT)/Φ(LE), which is larger for FPP4C (3.3) than for PP4C (1.5), see Figure 2 and Table 2, indicating that there is less LE relative to ICT for FPP4C than with PP4C.

TABLE 6: Excited State Absorption (ESA) Maxima (334−1072 nm) for FPP4C and PP4C in *n*-Hexane and Acetonitrile (MeCN) at 290 nm Excitation (Figures 10–15)

	ESA maxima [nm]	
	n-hexane	MeCN
FPP4C	444, 699	377, 499
PP4C	378, 444, 729	453, below 334
DMABN (LE)[a]	300−320, 445, 745	320, 355, 440, 710
DMABN (ICT)[a]	−	315, 425
NTC6 (LE)[b]	470,[c] 800[c]	
NTC6 (ICT)[b]		below 334,[d] 435[d]

[a] Data from ref 31. [b] Data from ref 15. [c] At a 0.2 ps pump−probe delay time. [d] At a 5 ps delay time.

Transient Absorption Spectra of FPP4C in Acetonitrile. The transient absorption spectrum of FPP4C in MeCN at a pump−probe delay time of 70 fs (Figure 12a) consists of a main band at around 400 nm and a weaker broad absorption at around 700 nm. By subtracting the SE (only ICT in MeCN, Figure 4c), the ESA spectrum in Figure 12b is obtained. With increasing delay time, the SE band of FPP4C in MeCN undergoes a shift to longer wavelengths, from 360.0 nm at $t = 0$ to 477 nm at $t = \infty$ (Figure 12b). This shift is simulated by adopting for the SE band in MeCN at time zero that of FPP4C in *n*-hexane (corrected for the difference between the absorption spectra in this solvent and in MeCN) and for the band at infinite time the SE spectrum in MeCN.[81] The time development between these extremes is taken from the time shift of the maximum $\tilde{\nu}$(ESA) between 408 and 377 nm, shown in Figure 12c. Decay times of 100 and 680 fs are obtained by fitting the shift of $\tilde{\nu}$(ESA) from 408 to 377 nm, employing eq 13, where ω^{-1} and τ_s are the Gaussian and diffusional solvation times.[82]

$$\tilde{\nu}^{max}(t) = \tilde{\nu}^{max}(\infty) + a_1\exp(-\omega^2 t^2/2) + a_2\exp(-t/\tau_s) \quad (13)$$

The ICT ESA spectrum of FPP4C in MeCN at a 70 fs pump−probe delay time has maxima at 405 and 665 nm, which

shift to 380 and 500 nm at a 5 ps delay (Figure 12b). The ESA spectrum does not change further between delays of 2 and 120 ps, with the same clear maxima at 380 and 500 nm (Figure 13b). The spectrum is that of the equilibrated ICT state. From 2 to 120 ps delay, no absorption maximum is observed at around 700 nm, attrubuted to LE (Figures 12b and S3). The maximum at 500 nm persists to a delay of 120 ps.

The band integral BI(580,1030) of FPP4C in MeCN displays a double exponential decay (Figure 12d), with a shortest decay time of $\tau_{i2} = 87$ fs and a longer time of $\tau_{i1} = 890$ fs, both times being much shorter than the ICT lifetime τ'_o(ICT) of 29.7 ns for FPP4C in MeCN at 25 °C (Table 5). This shows that the ICT reaction of FPP4C is ultrafast, limited by the main component of the dielectric relaxation time of 89 and 630 fs measured for MeCN.[31,83] A similar ultrafast ICT reaction governed by solvent relaxation was found in the ESA spectra of a series of 2,3,5,6-tetrafluoroaminobenzonitriles XABN4F, likewise having a shortest decay of around 90 fs in MeCN.[33] The longer time τ_{i1} of 890 fs in Figure 12d could also be due to solvent relaxation.[83] BI(340,410) in the ESA spectrum grows in with similar times, 90 fs and 1.3 ps.

Transient Absorption Spectra of PP4C in MeCN. The transient absorption and ESA spectra of PP4C in MeCN (Figure 14) are similar to those of FPP4C in this solvent; see Figure 12. The ESA spectra in Figure 14b are obtained by subtraction of the SE spectra, which show a spectral shift from 347 nm at $t = 0$ to 498 nm at $t = \infty$ (Figure 14b), employing the same procedure as described for Figure 12. At a pump−probe delay time of 70 fs, the ESA spectrum has a long-wavelength maximum at around 750 nm, shifting to 455 nm (shoulder) at a delay of 5 ps (Figures 14b). For delay times between 2 and 120 ps, the ESA spectrum of PP4C in MeCN remains unchanged, with maxima at 455 nm (shoulder) and below 334 nm (Figure 15b). This spectrum is again that of the relaxed ICT state. As compared with FPP4C (Figure 12b), however, the spectral band below 500 nm (Figure 14b) is broader and shows a horizontal shift to shorter wavelengths, from 425 nm at 70 fs to below 334 nm at a 5 ps delay.

The decay of the band integral BI(600,1040) is double exponential (Figure 14c), with a shortest decay time of $\tau_{i2} = 67$ fs and a longer time of $\tau_{i1} = 360$ fs, both times being again much shorter than the ICT lifetime τ'_o(ICT) of 13.6 ns for PP4C in MeCN at 25 °C (Table 5). The two decay times τ_{i2} and τ_{i1} are related to the dielectric relaxation times of MeCN (89 and

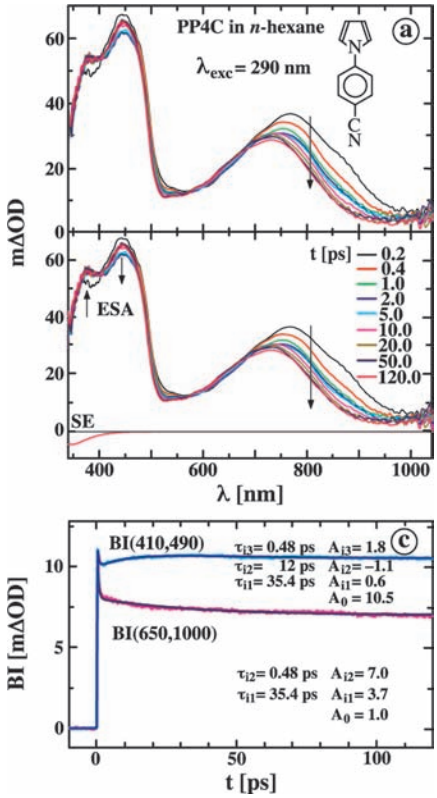

Figure 11. 4-Cyano-*N*-phenylpyrrole (PP4C) in *n*-hexane at 290 nm excitation. (a) Transient absorption spectra and (b) excited-state absorption (ESA) spectra after subtraction of the stimulated emission (SE), at pump−probe delay times between 0.2 and 120 ps. The SE spectrum (LE and ICT, cf. Figure 2c) is also depicted. In (b), the downward arrows (805 and 444 nm) indicate the decay of the LE absorption, whereas the upward arrow (378 nm) shows the rise of the ICT absorption. (c) Decay curves of the band integrals BI(410,490) and BI(650,1000). See the caption of Figure 10.

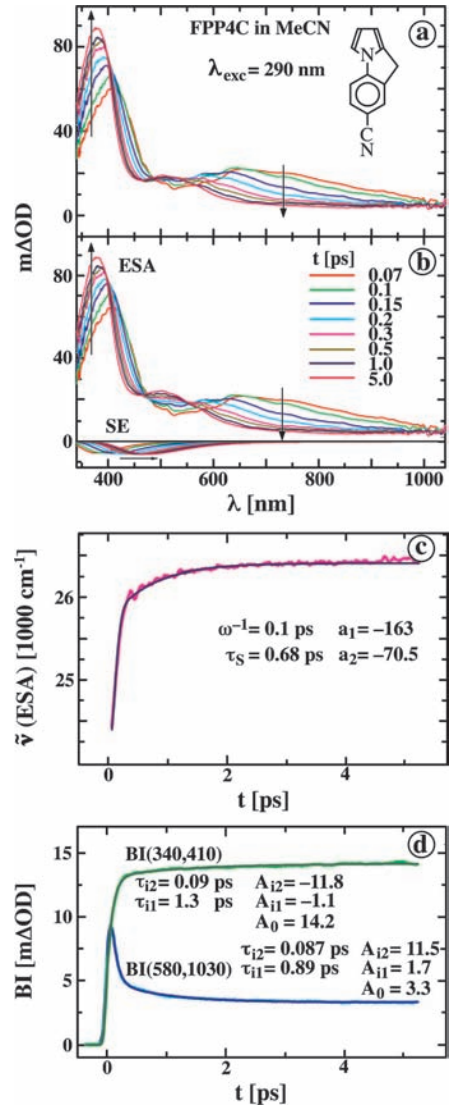

Figure 12. 4-Cyanofluorazene (FPP4C) in acetonitrile (MeCN) at 290 nm excitation. (a) Transient absorption spectra and (b) excited-state absorption (ESA) spectra after subtraction of the stimulated emission (SE), at pump−probe delay times between 0.07 and 5.0 ps. The spectral time shift of the ICT SE spectrum is also shown. In (b), the downward arrow (730 nm) indicates the decay of the LE absorption, whereas the upward arrow (below 400 nm) represents the rise of the ICT absorption. (c) The shift of the maximum of the ESA band at around 400 nm (from 408 to 377 nm, Figure 12 b) is fitted by using eq 13. (d) Double exponential decay curve of the band integrals BI(340,410) and BI(580,1030). See the caption of Figure 10.

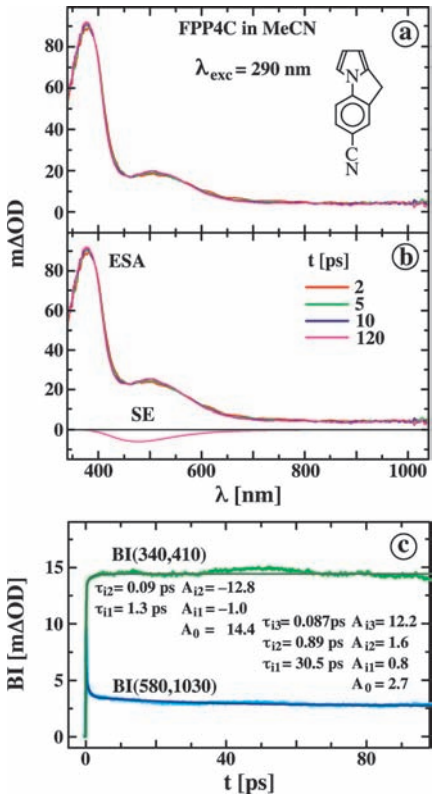

Figure 13. 4-Cyanofluorazene (FPP4C) in acetonitrile (MeCN) at 290 nm excitation. (a) Transient absorption spectra and (b) excited-state absorption (ESA) spectra after subtraction of the stimulated emission (SE), with pump−probe delay times between 2 and 120 ps. The ICT SE spectrum is also shown. (c) Analysis of the band integrals BI(340,410) and BI(580,310). See the caption of Figure 10.

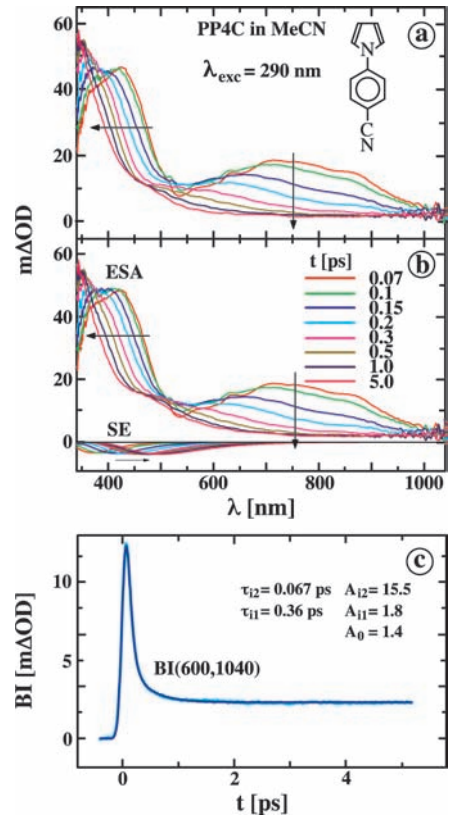

Figure 14. 4-Cyano-*N*-phenylpyrrole (PP4C) in acetonitrile (MeCN) at 290 nm excitation. (a) Transient absorption spectra and (b) excited-state absorption (ESA) spectra after subtraction of the stimulated emission (SE), at pump−probe delay times between 0.07 and 5.0 ps. The spectral time shift of the ICT SE spectrum is also shown. In (b), the downward arrow (755 nm) indicates the decay of the LE absorption. The band with a maximum at 425 nm for a 70 fs delay shifts to 338 nm at a 5 ps delay: horizontal arrow. (c) Decay curve of the band integral BI(600,1040). See the caption of Figure 10.

630 fs),[83] as discussed for FPP4C. From the decay of BI(600,1040) in Figure 15c, the two shortest times are the same as those in Figure 14c. For PP4C in MeCN with 266 nm excitation, similar ESA spectra are obtained (Figures S6 and S7).

Planar ICT Molecular Structure of FPP4C and PP4C. From the similarity of the photostationary absorption and fluorescence spectra (Figures 2–5), the ICT dipole moments μ_e(ICT) (Figure 6 and Table 4), the LE and ICT fluorescence decays (Figures 7 and 8), the radiative rate constants k'_f(ICT) (Table 5), and, in particular, the femtosecond transient absorption spectra (Figures 10–15), it is concluded that the ICT state of PP4C has the same planar structure as that of FPP4C, with a zero or small twist angle between the pyrrole and benzonitrile subgroups. It hence follows that a full perpendicular twist (TICT) of the pyrrole and benzonitrile subgroups in FPP4C and PP4C is not required for an efficient ICT reaction. A similar conclusion has been made for FPP[26] relative to PP as well as for NTC6[10,15] as compared with DMABN.

The planar ICT structure found here for FPP4C and PP4C corresponds to the Q state introduced by Haas and co-workers.[21,84] The perpendicularly twisted ICT configuration reported for PP4C in the literature was based on its assumedly small radiative rate constant k'_f(ICT),[25] which was shown here to be comparable to that of the planar FPP4C (Table 5).[14,72]

No Direct ICT Excitation for FPP4C and PP4C. From an analysis of the picosecond fluorescence and femtosecond ESA measurements of FPP4C and PP4C in *n*-hexane and MeCN, a conclusive differentiation between direct ICT excitation and excitation of LE as the precursor for ICT is problematic. The ESA spectra make clear that the ICT state of FPP4C and PP4C in both solvents is already populated to a large extent at 100 fs after excitation. The ICT reaction of these molecules is clearly much faster than that observed with most other dual fluorescent compounds, except for DTABN and mDTABN.[52] It is nevertheless concluded, that there is no direct ICT excitation with FPP4C and PP4C, a conclusion reached from a comparison with other A/D sytems in solution, such as DMABN and PP.

In the case of DMABN in MeCN, it follows from the observation of $A_{22}/A_{21} = -1.0$ (eq 8) that the ICT concentration at $t = 0$ is equal to zero, which means that direct ICT excitation did not occur; the ICT state is formed via the LE precursor.[31,59] Direct ICT excitation has also been shown to be absent for a large number of D/A molecules, such as FPP in EtCN,[26] PP in MeCN, EtCN, and PrCN,[20] DMABN in toluene,[13,65] DEE,[11] and 1,4-dioxane,[65] as well as 4-(diethylamino)benzonitrile (DEABN) in DEE,[85] 4-(di-*n*-propylamino)benzonitrile (DPrABN) in DEE,[11] DIABN in *n*-hexane,[63] NTC6 in *n*-hexane[15] and DEE,[10] 4-(*N*-azetidinyl)-3,5-dimethyl-benzonitrile (M4D) in DEE,[12] and the 4-dialkylamino-2,6-dimethylbenzonitriles MDB (methyl), EDB (ethyl), and PrDB (*n*-propyl) in toluene.[13] In support of these findings, it has been shown that LE is the ICT precursor for DMABN in THF as well as for DPrCF3 in MeCN, from the absence of an excitation wavelength dependence for S_1 and S_2 absorption, as mentioned above.[59]

The conclusion that LE is the ICT precursor is further strengthened by the condition that the FC state populated by ICT emission has an energy E(FC,ICT) of 89 kJ/mol above the

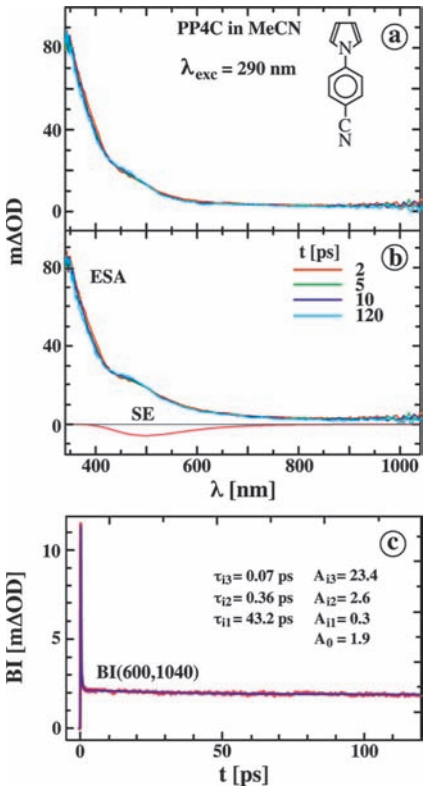

Figure 15. 4-Cyano-*N*-phenylpyrrole (PP4C) in acetonitrile (MeCN) at 290 nm excitation. (a) Transient absorption spectra and (b) excited-state absorption (ESA) spectra after subtraction of the stimulated emission (SE), at pump−probe delay times between 2 and 120 ps. The ICT SE spectrum is also shown. (c) Decay curve of the band integral BI(600,1040). See the caption of Figure 10.

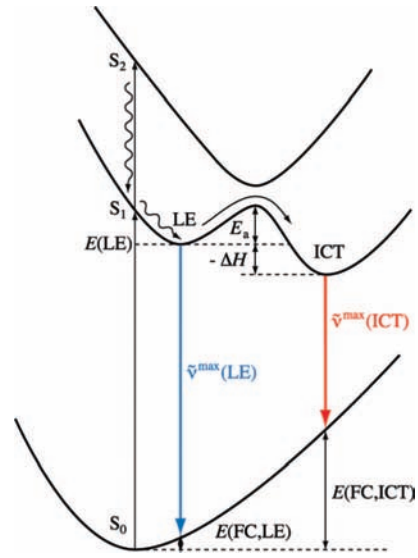

Figure 16. Potential energy surfaces for the ground state S_0 and the excited states S_1, S_2, LE, and ICT. When excited to the S_2 state (with an energy gap $\Delta E(S_1,S_2)$ above S_1), the system relaxes by internal conversion to the equilibrated LE state, having an energy E(LE) above S_0. The ICT reaction proceeds from the LE to the ICT state, with a reaction barrier E_a and an enthalpy difference ΔH. Fluorescence from the LE and ICT states, with emission maxima $\tilde{\nu}^{max}$(LE) and $\tilde{\nu}^{max}$(ICT), reaches the corresponding Franck−Condon states E(FC,LE) and E(FC,ICT).

equilibrated S_0,[31] which means, from a Boltzmann distribution point of view, that the vertical S_0(FC,ICT) → ICT transition is therefore not a realistic alternative pathway to bypass LE in the course of the ICT reaction. For FPP4C and PP4C in *n*-hexane, E(FC,ICT) equals 41 and 44 kJ/mol (Table 2), see Figure 16, which likewise makes a direct S_0(FC) → ICT excitation improbable for these molecules.

With PP4C in an argon matrix, direct ICT excitation has been reported for an excitation wavelength smaller than the energy $E(S_1)$ of the LE state.[58] It was also pointed out that under conditions where LE can be excited, the direct ICT pathway can be neglected and will also not be effective in solution.[58]

Conclusions

Whereas the pyrrole/phenyl twist angle θ of crystalline FPP4C is close to zero (1.0°), as expected, the experimental $\theta = 24°$ of PP4C is somewhat smaller than the computed angle (30.9°). From a comparison of the absorption spectra of PP4C and FPP4C in *n*-hexane, these molecules are effectively planar, which means that PP4C is much less twisted in solution than in the crystal.

The fluorescence spectrum of FPP4C in *n*-hexane consists of a dual LE and ICT emission, with a quantum yield ratio Φ'(ICT)/Φ(LE) of 3.3 at 25 °C, increasing to 68 at −95 °C. Similar spectra are obtained with PP4C, for which Φ'(ICT)/Φ(LE) likewise becomes larger upon cooling, from 1.5 at 25 °C to 11 at −95 °C. This observation indicates that both substances are under HTL conditions in *n*-hexane ($k_d \gg 1/\tau'_o$(ICT)), typical for D/A compounds with a small ICT stabilization enthalpy $-\Delta H$ (11 kJ/mol for FPP4C, 7 kJ/mol for PP4C). From the absorption spectra, it follows that the energy gap $\Delta E(S_1,S_2)$ of FPP4C and PP4C is substantially smaller than that of FPP and PP, which explains, within the context of the PICT model, the large increase in the efficiency of their ICT reactions.

A dipole moment of μ_e(ICT) = 14.8 D was determined for FPP4C by solvatochromic analysis, whereas from a plot of the $\tilde{\nu}^{max}$ (ICT) of FPP4C against those of DIABN, μ_e(ICT) = 15.7 D was calculated. These dipole moments are similar to the μ_e(ICT) = 16.3 D of PP4C, showing that the presence of the methylene bridge in FPP4C does not restrict the ICT reaction.

From the longest picosecond fluorescence decay times τ_1, equal to the ICT lifetime τ'_o(ICT), the radiative rate constants can be determined via k'_f(ICT) = Φ'(ICT)/τ'_o(ICT). FPP4C has relatively small k'_f(ICT) values, decreasing with solvent polarity from 1.62×10^7 s^{-1} in DBE to 0.85×10^7 s^{-1} in MeCN. For PP4C, similar data are observed, from 1.19×10^7 s^{-1} in DBE to 0.47×10^7 s^{-1} in MeCN. This similarity shows that the small k'_f(ICT) rate constants in the case of PP4C are not associated with a TICT state, as sometimes claimed, because the ICT state of FPP4C is certainly not twisted.

The femtosecond ESA spectra of FPP4C and PP4C in *n*-hexane consist of LE and ICT absorption bands with only little time development in the subpicosecond time range, which indicates that an ultrafast LE ↔ ICT equilibrium is established. The ESA spectra of FPP4C and PP4C in MeCN likewise show a rapid change between pump−probe time delays of 70 fs and 2 ps. The long-wavelength band with a maximum at around 700 nm at a 70 fs delay time decreases in optical density and shifts to shorter wavelengths during this time range, which may indicate LE decay and ICT absorption band relaxation. The decay times determined from the spectral band integrals, with a short time of around 80 fs and a longer time between 360 and 900 fs, are similar to the dielectric relaxation times of 89 and 630 fs of MeCN and hence do not directly reflect the intrinsic ICT reaction time. From the fluorescence and time-

resolved spectra, it is seen that the ICT reaction of FPP4C is similar to that observed with its flexible counterpart PP4C. It is concluded from this similarity that the ICT states of FPP4C and PP4C have the same planar structure. The presence of the rigidifying methylene bridge in FPP4C does not slow down the ICT reaction with respect to PP4C, as also observed with FPP compared with PP and NTC6 relative to DMABN. This makes clear that a perpendicular twist of the D and A subunits in a donor/acceptor molecule is not a requirement for efficient ICT in the excited state.

Acknowledgment. Many thanks are due to Prof. N. P. Ernsting (Humboldt University Berlin) for the use of the femtosecond absorption equipment in the investigations reported here. We are grateful to Mr. W. Bosch for the synthesis of FPP4C. We also thank Mr. J. Bienert for carrying out HPLC purifications and Mr. H. Lesche for technical support. Prof. Z. Cao (Xiamen) and Prof. X.-Y. Li (Chengdu) kindly informed us of the results of their calculations with FPP. Prof. D. Phillips (London), Prof. M. Maroncelli (University Park, PA), and Prof. Y. Haas (Jerusalem) are thanked for useful discussions. A.D. gratefully acknowledges the support of the Hungarian Science Foundation (OTKA ID No. 76278).

Supporting Information Available: Crystallographic data, fluorescence spectra, and transient absorption spectra. This material is available free of charge via the Internet at http://pubs.acs.org.

References and Notes

(1) Heine, A.; Herbst-Irmer, R.; Stalke, D.; Kühnle, W.; Zachariasse, K. A. *Acta Crystallogr., Sect. B* **1994**, *50*, 363.
(2) Jameson, G. B.; Sheikh-Ali, B. M.; Weiss, R. G. *Acta Crystallogr., Sect. B* **1994**, *50*, 703.
(3) Druzhinin, S. I.; Dix, I.; Mayer, P.; Noltemeyer, M.; Zachariasse, K. A. In preparation.
(4) Techert, S.; Zachariasse, K. A. *J. Am. Chem. Soc.* **2004**, *126*, 5593.
(5) Druzhinin, S. I.; Demeter, A.; Zachariasse, K. A. *Chem. Phys. Lett.* **2001**, *347*, 421.
(6) Braun, M.; v. Korff-Schmising, C.; Kiel, M.; Zhavoronkov, N.; Dreyer, J.; Bargheer, M.; Elsaesser, T.; Root, C.; Schrader, T. E.; Gilch, P.; Zinth, W.; Woerner, M. *Phys. Rev. Lett.* **2007**, *98*, 248301.
(7) Clark, J. L.; Miller, P. F.; Rumbles, G. *J. Phys. Chem. A* **1998**, *102*, 4428.
(8) Zander, Ch.; Drexhage, K. H. *Adv. Photochem.* **1995**, *20*, 59.
(9) Grabowski, Z. R.; Rotkiewicz, K.; Rettig, W. *Chem. Rev.* **2003**, *103*, 3899.
(10) Zachariasse, K. A.; Druzhinin, S. I.; Bosch, W.; Machinek, R. *J. Am. Chem. Soc.* **2004**, *126*, 1705.
(11) (a) Zachariasse, K. A; Grobys, M.; von der Haar, Th.; Hebecker, A; Il'ichev, Yu. V.; Jiang, Y.-B.; Morawski, O.; Kühnle, W. *J. Photochem. Photobiol. A: Chem.* **1996**, *102*, 59. (b) Erratum: Zachariasse, K. A.; Grobys, M.; von der Haar, Th.; Hebecker, A.; Il'ichev, Yu. V.; Jiang, Y.-B.; Morawski, O.; Kühnle, W. *J. Photochem. Photobiol. A: Chem.* **1998**, *115*, 259.
(12) Zachariasse, K. A.; Grobys, M.; von der Haar, Th.; Hebecker, A.; Il'ichev, Yu. V.; Morawski, O.; Rückert, I.; Kühnle, W. *J. Photochem. Photobiol. A: Chem.* **1997**, *105*, 373.
(13) Il'ichev, Yu. V.; Kühnle, W.; Zachariasse, K. A. *J. Phys. Chem. A* **1998**, *102*, 5670.
(14) Zachariasse, K. A. *Chem. Phys. Lett.* **2000**, *320*, 8.
(15) Druzhinin, S. I.; Kovalenko, S. A.; Senyushkina, T.; Zachariasse, K. A. *J. Phys. Chem. A* **2007**, *111*, 12878.
(16) Hättig, C.; Hellweg, A.; Köhn, A. *J. Am. Chem. Soc.* **2006**, *128*, 15672.
(17) Gómez, I.; Mercier, Y.; Reguero, M. *J. Phys. Chem. A* **2006**, *110*, 11455.
(18) Amatatsu, Y. *J. Phys. Chem. A* **2005**, *109*, 7225.
(19) Druzhinin, S. I.; Galievsky, V. A.; Yoshihara, T.; Zachariasse, K. A. *J. Phys. Chem. A* **2006**, *110*, 12760.
(20) Yoshihara, T.; Druzhinin, S. I.; Demeter, A.; Kocher, N.; Stalke, D.; Zachariasse, K. A. *J. Phys. Chem. A* **2005**, *109*, 1497.
(21) Zilberg, S.; Haas, Y. *J. Phys. Chem. A* **2002**, *106*, 1.
(22) Cornelissen-Gude, C.; Rettig, W. *J. Phys. Chem. A* **1998**, *102*, 7754.
(23) Okamoto, H.; Kinoshita, M. *J. Phys. Chem A* **2002**, *106*, 3485.
(24) Yoshihara, T.; Galievsky, V. A.; Druzhinin, S. I.; Saha, S.; Zachariasse, K. A. *Photochem. Photobiol. Sci.* **2003**, *2*, 342.
(25) Murali, S.; Rettig, W. *J. Phys. Chem. A* **2006**, *110*, 28.
(26) Yoshihara, T.; Druzhinin, S. I.; Zachariasse, K. A. *J. Am. Chem. Soc.* **2004**, *126*, 8535.
(27) Xu, X.; Cao, Z.; Zhang, Q. *J. Phys. Chem. A* **2006**, *110*, 1740.
(28) He, R.-X.; Li, X.-Y. *Chem. Phys.* **2007**, *332*, 325.
(29) Elming, N.; Clauson-Kaas, N. *Acta Chem. Scand.* **1952**, *6*, 867.
(30) Bailey, A. S.; Scott, P. W.; Vandrevala, M. H. *J. Chem. Soc., Perkin Trans. 1* **1980**, 97.
(31) Druzhinin, S. I.; Ernsting, N. P.; Kovalenko, S. A; Pérez Lustres, L.; Senyushkina, T.; Zachariasse, K. A. *J. Phys. Chem. A* **2006**, *110*, 2955.
(32) Demas, J. N.; Crosby, G. A. *J. Phys. Chem.* **1971**, *75*, 991.
(33) Galievsky, V. A.; Druzhinin, S. I.; Demeter, A.; Jiang, Y.-B.; Kovalenko, S. A.; Lustres, L. P.; Venugopal, K.; Ernsting, N. P.; Allonas, X.; Noltemeyer, M.; Machinek, R.; Zachariasse, K. A. *Chem. Phys. Chem.* **2005**, *6*, 2307.
(34) Kovalenko, S. A.; Dobryakov, A. L.; Ruthmann, J.; Ernsting, N. P. *Phys. Rev. A* **1999**, *59*, 2369.
(35) Ernsting, N. P.; Kovalenko, S. A.; Senyushkina, T. A.; Saam, J.; Farztdinov, V. *J. Phys. Chem. A* **2001**, *105*, 3443.
(36) von Bülow, R. Diplomarbeit (Master Thesis), University of Göttingen, 1996.
(37) Schweke, D.; Abramov, S.; Haas, Y. *Chem. Phys.* **2007**, *335*, 87.
(38) Earlier calculations on the molecular structure of *N*-phenylpyrrole (PP) are discussed in ref 20.
(39) Parusel, A. B. J. *Phys. Chem. Chem. Phys.* **2000**, *2*, 5545.
(40) van Bolhuis, F.; Kiers, C. Th. *Acta Crystallogr., Sect. B* **1978**, *34*, 1015.
(41) Liebman, J. F.; Skancke, A. *Mol. Phys.* **1997**, *91*, 471.
(42) Burgers, J.; Hoefnagel, M. A.; Verkade, P. E.; Visser, H.; Wepster, B. M. *Recl. Trav. Chim. Pays-Bas* **1958**, *77*, 491.
(43) Rückert, I.; Demeter, A.; Morawski, O.; Kühnle, W.; Tauer, E.; Zachariasse, K. A. *J. Phys. Chem. A* **1999**, *103*, 1958.
(44) Rückert, I.; Hebecker, A.; Parusel, A. B. J.; Zachariasse, K. A. *Z. Phys. Chem.* **2000**, *214*, 1597.
(45) Rettig, W.; Marschner, F. *Nouv. J. Chim.* **1983**, *7*, 425.
(46) Rettig, W.; Marschner, F. *New J. Chem.* **1990**, *14*, 819.
(47) Lumbroso, H.; Bertin, M.; Marschner, F. *J. Mol. Struct.* **1988**, *178*, 187.
(48) Birks, J. B. *Photophysics of Aromatic Molecules*; Wiley: London, 1970.
(49) Berlman, I. B. *Handbook of Fluorescence Spectra of Aromatic Molecules*; Academic Press: New York, 1971.
(50) Murali, S.; Changenet-Barret, P.; Ley, C.; Plaza, P.; Rettig, W.; Martin, M. M.; Lapouyade, R. *Chem. Phys. Lett.* **2005**, *411*, 192.
(51) Murali, S.; Kharlanov, V.; Rettig, W.; Tolmachev, A. I.; Kropachev, A. V. *J. Phys. Chem. A* **2005**, *109*, 6420.
(52) Druzhinin, S. I.; Dubbaka, S. R.; Knochel, P.; Kovalenko, S. A.; Mayer, P.; Senyushkina, T.; Zachariasse, K. A. *J. Phys. Chem. A* **2008**, *112*, 2749.
(53) Daum, R.; Druzhinin, S.; Ernst, D.; Rupp, L.; Schroeder, J.; Zachariasse, K. A. *Chem. Phys. Lett.* **2001**, *341*, 272.
(54) Il'ichev, Yu. V.; Kühnle, W.; Zachariasse, K. A. *Chem. Phys.* **1996**, *211*, 441.
(55) Arzhantsev, S.; Zachariasse, K. A.; Maroncelli, M. *J. Phys. Chem. A* **2006**, *110*, 3454.
(56) Kovalenko, S. A.; Schanz, R.; Senyushkina, T. A.; Ernsting, N. P. *Phys. Chem. Chem. Phys.* **2002**, *4*, 703.
(57) Ernsting, N. P; Breffke, J.; Vorobyev, D. Yu.; Duncan, D. A.; Pfeffer, I. *Phys. Chem. Chem. Phys.* **2008**, *10*, 2043.
(58) Schweke, D.; Baumgarten, H.; Haas, Y.; Rettig, W.; Dick, B. *J. Phys. Chem. A* **2005**, *109*, 576.
(59) Galievsky, V. A.; Zachariasse, K. A. *Acta Phys. Pol., A* **2007**, *112*, S-39.
(60) Suppan, P.; Ghoneim, N. *Solvatochromism*; The Royal Society of Chemistry: Cambridge, U.K., 1997.
(61) Liptay, W. In *Excited States*; Lim, E. C, Ed.; Academic Press: New York, 1974; Vol. 1, p 129.
(62) Baumann, W.; Bischof, H.; Brittinger, J.-C.; Rettig, W.; Rotkiewicz, K. *J. Photochem. Photobiol. A: Chem.* **1992**, *64*, 49.
(63) Demeter, A.; Druzhinin, S.; George, M.; Haselbach, E.; Roulin, J.-L.; Zachariasse, K. A. *Chem. Phys. Lett.* **2000**, *323*, 351.
(64) Schuddeboom, W.; Jonker, S. A.; Warman, J. M.; Leinhos, U.; Kühnle, W.; Zachariasse, K. A. *J. Phys. Chem.* **1992**, *96*, 10809.
(65) Leinhos, U.; Kühnle, W.; Zachariasse, K. A. *J. Phys. Chem.* **1991**, *95*, 2013.
(66) Lahmani, F.; Zehnacker-Rentien, A.; Coudert, L. H.; Zachariasse, K. A. *J. Phys. Chem. A* **2003**, *107*, 7364.
(67) Suzuki, K.; Demeter, A.; Kühnle, W.; Tauer, E.; Zachariasse, K. A.; Tobita, S.; Shizuka, H. *Phys. Chem. Chem. Phys.* **2000**, *2*, 981.

(68) The simplified expression $k'_f(\mathrm{ICT}) = \Phi'(\mathrm{ICT})/\tau'_o(\mathrm{ICT})$ (eq 9) is valid when $1/\tau'_o(\mathrm{ICT}) \gg F$, where $F = 1/\tau_o(\mathrm{LE})\,[(k_d + 1/\tau'_o(\mathrm{ICT}))/k_a]$; see eq 10 (ref 20). This is hence the case when $1/\tau'_o(\mathrm{ICT}) \gg 1/\tau_o(\mathrm{LE})k_d/k_a$ or when $k_a/k_d \gg \tau'_o(\mathrm{ICT})/\tau_o(\mathrm{LE})$ in the HTL limit ($k_d \gg 1/\tau'_o(\mathrm{ICT})$). This means that under normal conditions, where $\tau'_o(\mathrm{ICT})$ has the same order of magnitude as $\tau_o(\mathrm{LE})$ (ref 31), eq 9 is valid when k_a/k_d, the equilibrium constant K of the ICT reaction, is much larger than 1, that is, when the equilibrium is strongly shifted toward the ICT state. On the other hand, for an ICT reaction under LTL conditions ($k_d \ll 1/\tau'_o(\mathrm{ICT})$), the conceptually simple situation of an irreversible LE → ICT reaction, eq 9, is generally valid, provided that $k_a \gg 1/\tau_o(\mathrm{LE})$ or $k_a\tau_o(\mathrm{LE}) \gg 1$. It should be noted that the value of the ICT enthalpy difference $-\Delta H$ determines whether HTL (small $-\Delta H$) or LTL (large $-\Delta H$) conditions prevail (ref 13).

(69) Beens, H.; Weller, A. In *Organic Molecular Photophysics*; Birks, J. B., Ed.; Wiley: London, 1975; Vol. 2, Chapter 4.

(70) Hirayama, S.; Phillips, D. *J. Photochem.* **1980**, *12*, 139.

(71) Toptygin, D. *J. Fluoresc.* **2003**, *13*, 201.

(72) Okada, T.; Uesugi, M.; Köhler, G.; Rechthaler, K.; Rotkiewicz, K.; Rettig, W.; Grabner, G. *Chem. Phys.* **1999**, *241*, 327.

(73) Druzhinin, S. I; Kovalenko, S. A.; Senyushkina, T.; Zachariasse, K. A. In preparation.

(74) Reichhardt, Ch.; Zachariasse, K. A.; Schwarzer, D. In preparation.

(75) Okamoto, H.; Inishi, H.; Nakamura, Y.; Kohtani, S.; Nakagaki, R. *J. Phys. Chem. A* **2001**, *105*, 4182.

(76) Ma, C.; Kwok, W. M.; Matousek, P.; Parker, A. W.; Phillips, D.; Toner, W. T.; Towrie, M. *J. Phys. Chem. A* **2002**, *106*, 3294.

(77) Demeter, A.; Zachariasse, K. A. *J. Phys. Chem. A* **2008**, *112*, 1359.

(78) Agmon, N. *J. Phys. Chem.* **1990**, *94*, 2959.

(79) Karunakaran, V.; Senyushkina, T.; Saroja, G.; Liebscher, J.; Ernsting, N. P. *J. Phys. Chem. A* **2007**, *111*, 10944.

(80) Abramov, S.; Schweke, D.; Zilberg, S.; Haas, Y. *Chem. Phys.* **2007**, *335*, 79.

(81) Fee, R. S.; Maroncelli, M. *Chem. Phys.* **1994**, *183*, 235.

(82) Pérez Lustres, J. L.; Rodriguez-Prieto, F.; Mosquera, M.; Senyushkina, T. A.; Ernsting, N. P.; Kovalenko, S. A. *J. Am. Chem. Soc.* **2007**, *129*, 5408.

(83) Horng, M. L.; Gardecki, J. A.; Papazyan, A.; Maroncelli, M. *J. Phys. Chem.* **1995**, *99*, 17311.

(84) Cogan, S.; Zilberg, S.; Haas, Y. *J. Am. Chem. Soc.* **2006**, *128*, 3335.

(85) von der Haar, Th.; Hebecker, A.; Il'ichev, Yu.; Kühnle, W.; Zachariasse, K. A. In *Fast Elementary Processes in Chemical and Biological Systems*, Proceedings of the AIP Conference, Lille, France, 1995; AIP Press: Woodbury, NY, 1996; Vol. 364, p 295.

JP8037413